



**CHALMERS**  
UNIVERSITY OF TECHNOLOGY

---

# **Trajectory Planning for Automated Driving of Articulated Heavy Vehicles**

Using model predictive control

Master's thesis in Systems, Control and Mechatronics

JULIUS DIESTRA

SPYRIDON SKOURAS

---

Department of Electrical Engineering  
CHALMERS UNIVERSITY OF TECHNOLOGY  
Gothenburg, Sweden 2019



MASTER'S THESIS 2019:NN

# Trajectory Planning for Automated Driving of Articulated Heavy Vehicles

Using model predictive control

JULIUS DIESTRA SPYRIDON SKOURAS



**CHALMERS**  
UNIVERSITY OF TECHNOLOGY

Department of Electrical Engineering  
*Division of Systems and Control*  
CHALMERS UNIVERSITY OF TECHNOLOGY  
Gothenburg, Sweden 2019

Trajectory Planning for Automated Driving of Articulated Heavy Vehicles  
Using model predictive control  
JULIUS DIESTRA SPYRIDON SKOURAS

© JULIUS DIESTRA, SPYRIDON SKOURAS, 2019.

Supervisor: Peter Nilsson and Patrik Nilsson, Volvo AB  
Examiner: Jonas Fredriksson, Chalmers, Systems and Control

Master's Thesis 2019:NN  
Department of Electrical Engineering  
Division of Systems and Control  
Chalmers University of Technology  
SE-412 96 Gothenburg  
Telephone +46 31 772 1000

Typeset in L<sup>A</sup>T<sub>E</sub>X  
Printed by Chalmers Reproservice  
Gothenburg, Sweden 2019

Trajectory Planning for Automated Driving of Articulated Heavy Vehicles  
Using model predictive control  
JULIUS DIESTRA SPYRIDON SKOURAS  
Department of Electrical Engineering  
Chalmers University of Technology

## Abstract

Automotive industries have shown great interest in designing autonomous heavy vehicles in the last decades. Hence, the role of the driver will belong to the past in the close future and control functions will handle their tasks. However, the development of control functions for maneuvering is a challenging area of research due to the size and motion characteristics of the heavy vehicles.

This project is focused on designing trajectory planners for a truck with a semi-trailer. Since the aim of the planners is to make possible for the vehicle to cross sharp corners and roundabouts, the design is restricted in low velocities. The generated trajectories satisfy also some additional constraints, which are related to good performance and safety.

The method used for the generation of such trajectories is based on numerical optimization and more specifically model predictive control. The selection of the method can be explained by the fact that it solves optimization problems considering constraints. The software tool used to solve the optimization problems is Forces Pro.

In this study, three different trajectory planners are developed and tested. Each planner is based on different equations describing the motion of the vehicle such as the kinematics and dynamics. For all of the planners, the prediction horizon is selected to be 8 seconds. The trajectory planners are also tested with a high fidelity model (provided by Volvo GTT) in a real-time simulation environment.

Lastly, it can be observed from the results that all planners manage to generate smooth and safe trajectories, making it possible at the same time for the truck to cross two sharp corners and a roundabout in a satisfying manner.

Keywords: Model predictive control, trajectory planning, semi-trailer combination, optimization, modelling, Matlab/Simulink, Forces Pro.



# Acknowledgements

We would like to thank our supervisors from Volvo GTT Peter Nilsson and Patrik Nilsson for supporting us during the conduction of this master thesis. Through their experience and knowledge, they helped us overcome obstacles and learn from them. Lastly, we would like to thank our supervisor from Chalmers University of Technology Jonas Fredriksson, who was always willing to help our work and provided us with useful advice.

Gothenburg, June 2019  
Chalmers University of Technology

Spyridon Skouras  
Julius Diestra



# Contents

<b>List of Figures</b>	<b>xi</b>
<b>List of Tables</b>	<b>xiii</b>
<b>1 Introduction</b>	<b>1</b>
1.1 Objective . . . . .	2
1.2 Prerequisites . . . . .	2
1.3 Limitations . . . . .	3
1.4 Outline of the thesis . . . . .	3
<b>2 Background</b>	<b>5</b>
2.1 Definitions . . . . .	5
2.2 Trajectory planning techniques . . . . .	5
2.3 Trajectory planning for articulated heavy vehicles . . . . .	6
2.4 Motion characteristics of articulated vehicles . . . . .	7
2.5 Optimization problem . . . . .	8
2.6 State-space model . . . . .	9
2.7 Model predictive control . . . . .	10
<b>3 Modelling</b>	<b>13</b>
3.1 Road modeling . . . . .	13
3.2 Vehicle motion modeling . . . . .	14
3.2.1 System description . . . . .	14
3.2.2 Rotation matrices . . . . .	15
3.2.3 Euler-Lagrange equation . . . . .	16
3.2.3.1 Generalized coordinates . . . . .	18
3.2.3.2 Kinetic energy . . . . .	19
3.2.3.3 Generalized forces . . . . .	19
3.3 Vehicle motion in road coordinates . . . . .	21
3.4 Nonlinear state-space model: Lateral and longitudinal dynamics . . . . .	25
3.5 Nonlinear state-space model: Only lateral dynamics . . . . .	26
3.6 Linear model: Lateral and longitudinal dynamics . . . . .	27
3.7 Linear model: Lateral dynamics . . . . .	28
3.8 Kinematic model . . . . .	29
3.9 Summary . . . . .	31
<b>4 Proposed trajectory planning system</b>	<b>33</b>

4.1	Longitudinal and lateral trajectory planner . . . . .	33
4.2	Lateral trajectory planner . . . . .	35
<b>5</b>	<b>Results</b>	<b>37</b>
5.1	Cornering stiffness estimation . . . . .	37
5.2	Model validation . . . . .	39
5.2.1	Model validation: Constant steering angle . . . . .	40
5.2.2	Model validation: Sinusoidal steering angle . . . . .	41
5.3	Trajectory planner: Simulations using Forces Pro solver and nonlinear state-space model . . . . .	43
5.4	Trajectory planner: Real time simulations using Forces Pro solver and HF model . . . . .	47
<b>6</b>	<b>Conclusions and Future work</b>	<b>53</b>
6.1	Conclusions . . . . .	53
6.2	Future work . . . . .	54
	<b>Bibliography</b>	<b>55</b>
<b>A</b>	<b>Nomenclature</b>	<b>I</b>

# List of Figures

1.1	Semi-trailer truck, reproduced from [1]. . . . .	1
1.2	Schematic architecture of an automated vehicle, reproduced from [9].	2
2.1	Truck with a semi trailer - Cornering Case - low speed, reproduced from [20]. . . . .	7
2.2	Rearward amplification for an A-double combination, reproduced from [22]. . . . .	8
2.3	Truck with a semi trailer - Cornering Case - high speed, reproduced from [22]. . . . .	8
2.4	Model predictive control algorithm. . . . .	11
3.1	Road model parameters. . . . .	14
3.2	Semi-trailer combination [51]. . . . .	15
3.3	Two-track model with multiple non-steerable axles and dual tyres. . .	15
3.4	One-track model with multiple non-steerable axles and single tyres. .	15
3.5	One-track model of a semi-trailer combination. . . . .	16
3.6	One-track model : Position vectors. . . . .	17
3.7	One-track model : Forces. . . . .	18
3.8	Semi-trailer motion relative to the road. . . . .	22
3.9	Road and its parameters. . . . .	23
3.10	Sigmoid function. . . . .	24
3.11	A set of four subfigures. . . . .	24
3.12	Modeling procedure summary. . . . .	32
4.1	Diagram of the longitudinal and lateral trajectory planner in the system.	34
4.2	Diagram of the lateral trajectory planner in the system. . . . .	35
5.1	Cornering stiffness of unit 1. . . . .	38
5.2	Cornering stiffness of unit 2. . . . .	38
5.3	Model validation diagram. . . . .	39
5.4	Center of gravity of vehicle unit 1 and 2. Input $\dot{\delta}_{11}(t) = 0$ and initial condition $\delta_{110} = 5^\circ$ . . . . .	40
5.5	Error estimation of the center of gravity of vehicle unit 1 and 2 by the nonlinear and linear mode. Input $\dot{\delta}_{11}(t) = 0$ and initial condition $\delta_{110} = 5^\circ$ . . . . .	41
5.6	Estimation of $\psi_1$ and $\Delta\psi_1$ . Input $\dot{\delta}_{11}(t) = 0$ and initial condition $\delta_{110} = 5^\circ$ . . . . .	41

5.7	Center of gravity of vehicle unit 1 and 2. Input $\dot{\delta}_{11}(t) = A \cdot \cos 2\pi \cdot f \cdot t$ and initial condition $\delta_{110} = 0^\circ$ . $A = 0.1053 \text{ rad/s}$ and $f = 0.08 \text{ Hz}$ . . . . .	42
5.8	Error estimation of the center of gravity of vehicle unit 1 and 2 by the nonlinear and linear mode. Input $\dot{\delta}_{11}(t) = A \cdot \cos 2\pi \cdot f \cdot t$ and initial condition $\delta_{110} = 0^\circ$ . $A = 0.1053 \text{ rad/s}$ and $f = 0.08 \text{ Hz}$ . . . . .	42
5.9	Estimation of $\psi_1$ and $\Delta\psi_1$ . Input $\dot{\delta}_{11}(t) = A \cdot \cos 2\pi \cdot f \cdot t$ and initial condition $\delta_{110} = 0^\circ$ . $A = 0.1053 \text{ rad/s}$ and $f = 0.08 \text{ Hz}$ . . . . .	42
5.10	A set of four subfigures. . . . .	45
5.11	A set of four subfigures. . . . .	46
5.12	Simulation using nonlinear model and Forces Pro: Planner solving time. . . . .	47
5.13	A set of four subfigures. . . . .	48
5.14	A set of four subfigures. . . . .	49
5.15	A set of four subfigures. . . . .	50
5.16	Real time simulation using HF model, Forces Pro and ROS: Planner solving time. . . . .	51

# List of Tables

5.1	Cornering stiffness estimated parameters. . . . .	39
5.2	Values of $T_s$ and $T_\Delta$ for each planner. . . . .	43
5.3	Lateral trajectory planners: Tuning parameters and boundaries. . . .	43
5.4	Trajectory planner using linear longitudinal and lateral dynamics model: Tuning parameters and boundaries. . . . .	44



# 1

## Introduction

During the last decades, automotive industries have shown a lot of interest in developing automated vehicles, see e.g. [2],[3],[4]. Even though, there is a lot of work needed in order for autonomous vehicles to replace the existing cars and trucks, experimental autonomous vehicles exist and are tested. The reason why automotive industries tend to develop automated vehicles can be seen by several advantages, some of them will be shortly mentioned below. According to [5], automated vehicles could have a positive impact on traffic safety. More specifically human errors are responsible for the highest percentage of car accidents [6]. Hence automated vehicles aim at making transportation safer. Furthermore, automated vehicles could limit the  $CO_2$  emissions. Truck platooning for aerodynamic drag reduction as well as employing the most efficient driving speeds could result to less emissions and as a result, automated vehicles could make transportation more environmental friendly [7]. Automated vehicles could also impact traffic congestions. In [8], researchers showed that autonomous vehicles managed to increase the traffic flow. This could have a strong impact to people's lives, as it would be much easier for people to manage their schedules at both personal lives and work.

This master thesis is focused on an automated driving system for a tractor semi-trailer combination, see Fig 1.1. The main goal is to design a trajectory planner that will generate a safe trajectory and at the same time guarantee maneuverability at low speeds. The planner is to be tested in simulation using a high - fidelity truck model in simulink.



**Figure 1.1:** Semi-trailer truck, reproduced from [1].

## 1.1 Objective

The main objective is to develop a trajectory planner, so that the vehicle combination can manoeuvre with respect to safety and efficiency. The trajectory planner should be as fast as possible and make it possible for the vehicle combination, to make sharp turns and negotiate roundabouts.

Model predictive control (MPC) method is selected for this purpose. In order to accomplish the main objective, the steps below are needed:

- modeling of the truck with a semi-trailer,
- verification of the above model, by comparing it with the high-fidelity truck model,
- development of a trajectory planner,
- trajectory planner test on the high-fidelity model.

## 1.2 Prerequisites

Trajectory planning is a one of the main functions for an automated vehicle Fig. 1.2. Though in order to for the reader to obtain a general view of the total structure, the rest of the the functionalities will be shortly explained. Firstly, the vehicle is equipped with sensor systems which provide information regarding the positions, velocities ,and orientations of the vehicle. Secondly, the prediction systems estimate the trajectories of the surrounding vehicles, while the decision making functionality is responsible for deciding when a manoeuvre should start. Then the trajectory planner is responsible for the generation of a smooth and safe for the vehicle trajectory. Lastly, the low level control systems are responsible for tracking the generated trajectory.

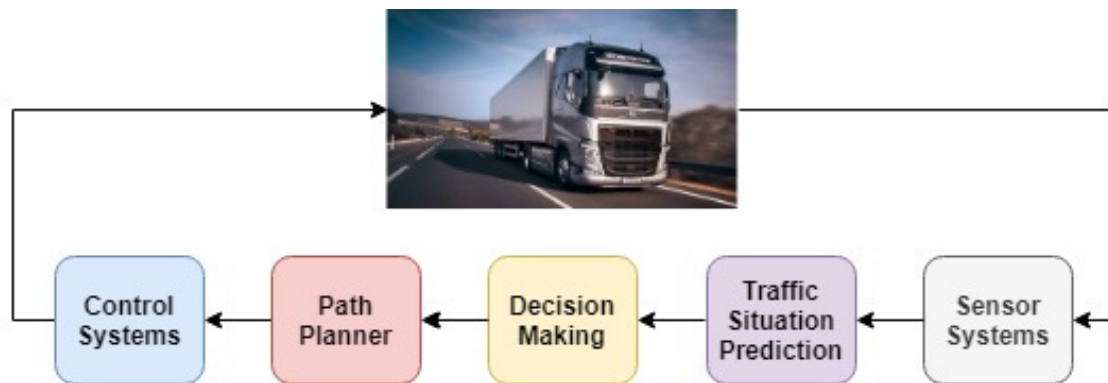


**Figure 1.2:** Schematic architecture of an automated vehicle, reproduced from [9].

Though, in this research, several assumptions are made, as far as these functions are concerned.

- All states information is available from already existing sensors and no further investigation is done on this topic.
- No surrounding vehicles and obstacles are considered in this research. Hence the traffic situation prediction is out of the scope of this thesis.

- No investigation is done on decision making.
- Actuation controls such as propulsion force, steering angle, and steering angle rate are assumed to be available for use.
- The road characteristics (curvature and angle of the road center line as well as road width) are known.

### 1.3 Limitations

In this subsection, several limitations of the designed trajectory planner are briefly presented.

- The following research is focused on a truck with semi-trailer. The trajectory planner is designed specifically for this type of truck combination.
- The trajectory planner is designed to operate at low velocities (below 20km/h).
- The trajectory planner is designed for a specific route, provided by Volvo GTT.

### 1.4 Outline of the thesis

**Chapter 2** In chapter 2, the background of this research is presented. Firstly several trajectory planning algorithms are briefly presented. The trajectory planning problem for automated heavy vehicles is described as well as previously researches on this topic are mentioned. Lastly, the definitions of optimization problem and state space representation of a model are explained.

**Chapter 3** Chapter 3 presents the equations describing the dynamics and kinematics of the truck with a semi-trailer. More specifically, the nonlinear dynamic model as well as a simplified version of the dynamic model is shown. Lastly, the kinematics's model equations are presented.

**Chapter 4** In chapter 4, the proposed trajectory planning algorithm is shown. More specifically, the selected optimization variables, cost function, and constraints of the optimization problem are presented.

**Chapter 5** Chapter 5 shows verification tests of each model, as well as the simulation results of the trajectory planner for each model. Lastly, simulation results with the high fidelity model are also presented.



# 2

## Background

In this chapter a brief description of several trajectory planning techniques used for automated heavy vehicles, are described. Also the characteristics of motion for heavy vehicles are shortly presented. Lastly brief definitions of the optimization problem, state space model and MPC are mentioned.

### 2.1 Definitions

According to the definitions, made in [1], a path is a geometric trace (including orientation) that a specific position of the vehicle, say, the centre of the first or the last vehicle axle, should follow whilst satisfying given constraints. Hence, the path planning problem is to find a path in the configuration space that starts at the initial configuration and reaches the target region whilst satisfying the given constraints. On the other hand, state trajectory can be interpreted as a generalisation of a path; prescribing the evolution of the states of a dynamic system in time. Finally, trajectory planning (also known as trajectory generation or motion planning) is a generalisation of path planning, involved with planning the state evolution in time while satisfying given constraints on the states and possibly the actuation.

### 2.2 Trajectory planning techniques

Various techniques have been published for autonomous vehicles for trajectory planning problems. These techniques can be classified in four groups: graph search, sampling, interpolating and numerical optimization [11].

- **Graph search.** The main goal of the graph search algorithms is to find the best path from an initial point A to a final point B. For that purpose, the state space is divided into grid cells. These algorithms visit every state in the grid and decide if there is a path to be followed (not necessarily optimal) or if there is no solution to the trajectory planning problem. The three following algorithms for graph search have been implemented in automated driving: Dijkstra algorithm, [12], A\* algorithm, [13] and state lattice algorithm, [14].
- **Sampling.** In sampling based algorithms, the state space is randomly divided into grid cells. A new cell is added into the graph if there is a path which connects that cell with an already existed cell in the graph. Finally, an optimal path is generated, connecting the start with the final point. The

main algorithms use in SBP are Rapidly-Exploring Random Tree (RRT) and Probabilistic Roadmap Method (PRM).

- **Curve Interpolating.** In general interpolation is the procedure in which given a set of data, a new set of data is calculated and inserted inside the old set (reference points). Interpolation curve planners generate smooth trajectories considering the vehicle constraints and changing surrounding environment. More specifically these algorithms consider the previous way points of a global road map and a new path is generated considering all limitations. Some of the most popular interpolation methods are lines and circles, clothoid curves, polynomial curves, spline curves and Bezier curves. Spline and clothoid methods and Bezier curves have been applied on automated driving, see e.g. [16] and [17].
- **Numerical Optimization.** The main goal in this method is the minimization of a cost function subject to several constraints of variables. Any specifications of an optimization problem could be included into the constraints. The cost function is weighted such that different variables of interest are penalized. In trajectory planning problems, the solution of an optimization problem could be path satisfying the desired requirements. Applications in automated driving can be found in [18]. It is worth mentioning that MPC is based on solving an optimization problem in each time instance.

### 2.3 Trajectory planning for articulated heavy vehicles

A lot of interest has appeared on trajectory planning for automated heavy vehicles, for both high-speed [22], [23] and [26] and low speed [25] scenarios, using MPC. In each scenario different formulation of the problem is used. At high speeds, the authors at [22], [23] and [26], are focused mostly on lane-changing. In these researches, after simplifications a linear model describing the motion of the vehicle, is used. An interesting approach is also the spatial formulation, which is used at [23] and [26]. On the other hand, at low speeds scenarios, the kinematic model is selected at [24] and [25], which shows good approximation in low velocities. The latter formulation leads to a nonlinear state space model, but much simpler than the nonlinear model describing the complete dynamics. The reason why different models are used in each scenario, is the fact that the complete differential equations describing the motion of the truck, are quite complex and contain many nonlinear terms. Hence the goal of the authors is to approximate the equations of motion of the heavy vehicle in each scenario with a simplified model. This goal has a strong impact on the feasibility and speed of the MPC algorithm. As mentioned before, the designed trajectory planner of this research is focused on maneuvering at low velocities. Both the kinematic and the dynamic models are considered as it will be seen at the next chapters. In a corner case (in which the truck maintains low speed), the truck is expected to deviate from the center of the road, so that the trailer will remain inside the road limits Fig. 2.1. Hence the trajectory planner is expected to generate a similar trajectory, considering at the same time the mechan-

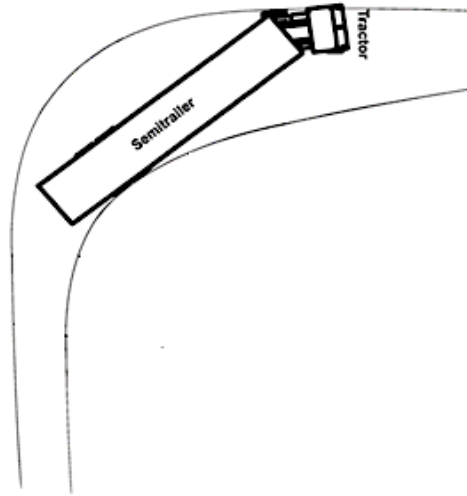


**Figure 2.1:** Truck with a semi trailer - Cornering Case - low speed, reproduced from [20].

ical limitations of the vehicle. Meanwhile the trajectory planners are designed for a specific route (provided by Volvo GTT). Defining the route outside the road limits as the obstacles and considering the above mentioned, the trajectory planning problem for automated heavy vehicles is described according to the trajectory planning definition.

## 2.4 Motion characteristics of articulated vehicles

There are two lateral phenomena occurring due to the length of a heavy truck at lane changing and cornering scenarios. These phenomena are the rearward amplification and the lateral off-tracking. During a maneuver, the rearward amplification can be observed, when the magnitude of the oscillation of the lateral acceleration of the last unit of a heavy vehicle combination is larger than the lateral acceleration magnitude of the truck, see illustration in Fig. 2.2. Hence, rearward amplification can lead to roll over. Rearward amplification its more visible at high speed maneuvering. Lateral off-tracking can be seen by the different trajectories that the front axle and the most rear axle follow when driving in a curve. At low velocities, the last unit tends to move inwards from the curve Fig. 2.1, whereas at high velocities the most rear position of the trailer, tends to move outwards Fig. 2.3.

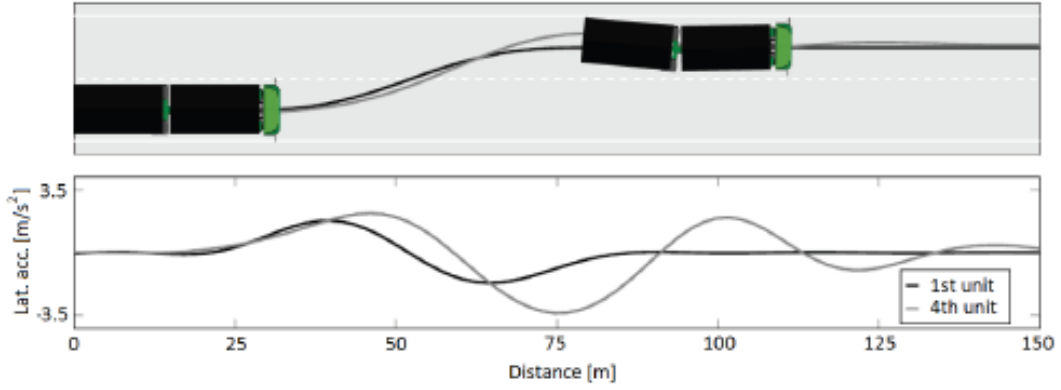


**Figure 2.2:** Rearward amplification for an A-double combination, reproduced from [22].

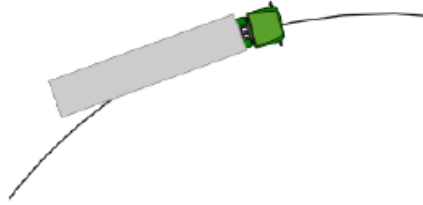


**Figure 2.3:** Truck with a semi trailer - Cornering Case - high speed, reproduced from [22].

## 2.5 Optimization problem

An optimization problem can be formulated as [27],

$$\begin{aligned}
 & \underset{z}{\text{minimize}} && J(z) \\
 & \text{subject to} && h_i(z) = 0 \quad \text{for } i \in \mathcal{E} \\
 & && g_i(z) \leq 0 \quad \text{for } i \in \mathcal{I} \\
 & && z \in \mathcal{Z}
 \end{aligned} \tag{2.1}$$

- |  |  |
|--|--|
| $z \in \mathbb{R}^n$                                   | : Decision variable vector $z_j, j = 1, 2, \dots, n$ ; |
| $J : \mathbb{R}^n \rightarrow \mathbb{R} \cup \{\pm\}$ | : Objective function;                                  |
| $h_i : \mathbb{R}^n \rightarrow \mathbb{R}$            | : Equality constraint defining restriction on $z$ ;    |
| $g_i : \mathbb{R}^n \rightarrow \mathbb{R}$            | : Inequality constraint defining restriction on $z$ ;  |
| $\mathcal{Z} \subseteq \mathbb{R}^n$                   | : Set defined by the lower and upper bounds on $z$ ;   |
| $\mathcal{E} = \{1, \dots, m\}$                        | : Set of number of equality constraints;               |
| $\mathcal{I} = \{1, \dots, l\}$                        | : Set of number of inequality constraints.             |

The feasible set ( $\mathcal{S} \subseteq \mathbb{R}^n$ ) is defined as the solution set of all the constraints of the system,

$$\mathcal{S} = \{z \in \mathbb{R}^n \mid h_i(z) = 0, i \in \mathcal{E}, g_i(z) \leq 0, i \in \mathcal{I}, z \in Z\} \quad (2.2)$$

A vector satisfying  $z \in \mathcal{S}$  is called a feasible solution. The feasible solution  $z^*$  which gives the objective function its minimal value among  $\mathcal{S}$  is called the optimal solution, [28],

$$J(z^*) \leq J(z) \quad , \quad z \in \mathcal{S} \quad (2.3)$$

The optimization problem (2.1) is denoted nonlinear when at least one of the functions  $J$ ,  $h_i$  or  $g_i$  is a nonlinear function. Moreover, when  $J$ ,  $h_i$  and  $g_i$  are linear functions, (2.1) is a linear optimization problem.

## 2.6 State-space model

A dynamic system can be described by the following differential equation [29],

$$\dot{x}(t) = f(x(t), u(t)) \quad , \quad x(0) = x_0 \quad (2.4)$$

where,

$x \in \mathbb{R}^n$	: State vector $x_j, j = 1, 2, \dots, n;$
$u \in \mathbb{R}^p$	: Input vector $u_j, j = 1, 2, \dots, p;$
$f : \mathbb{R}^n \times \mathbb{R}^p \rightarrow \mathbb{R}^n$	: Vector function $f_j, j = 1, 2, \dots, n;$
$x_0 \in \mathbb{R}^n$	: Initial state vector.

An equilibrium point  $(x_e, u_e)$  can be selected such that,

$$f(x_e, u_e) = 0 \quad (2.5)$$

Then, the nonlinear system can be linearized around the equilibrium point,

$$\dot{x}(t) = Ax(t) + Bu(t) \quad , \quad x(0) = x_0 \quad (2.6)$$

where,

$$A = \left. \frac{\partial f(x, u)}{\partial x} \right|_{(x_e, u_e)} \quad , \quad B = \left. \frac{\partial f(x, u)}{\partial u} \right|_{(x_e, u_e)} \quad (2.7)$$

The nonlinear and linear representations of the system can be sampled to obtain their discrete-time version [30]. In this document, the formulation of the discrete-time state-space model has the following form,

$$x(k+1) = f(x(k), u(k)) \quad (2.8)$$

where  $f$  can be a nonlinear or linear model. Moreover, the following notation will be used,

$$x_{k+j} = x(k+j) \quad , \quad j \in \mathbb{N} \quad (2.9)$$

## 2.7 Model predictive control

Model predictive control (MPC) uses the predicted behaviour of a system in a finite horizon to compute a control input sequence that optimize a cost function subject to constraints under the inputs and states of the system. The predicted behavior is obtained by using the system model, see [32] and [33].

In order to formulate the MPC algorithm, the following matrices are defined,

$$\bar{u} = \begin{pmatrix} u_k \\ u_{k+1} \\ \vdots \\ u_{k+N-1} \end{pmatrix} \quad (2.10)$$

$$\bar{x} = \begin{pmatrix} x_k \\ x_{k+1} \\ \vdots \\ x_{k+N} \end{pmatrix} \quad (2.11)$$

where  $N$  is the horizon,  $\bar{u}$  is the control input sequence and  $\bar{x}$  is the state sequence. The next step state sequence ( $\bar{x}^+$ ) can be defined as,

$$\bar{x}^+ = \begin{pmatrix} x_{k+1} \\ x_{k+2} \\ \vdots \\ x_{k+N} \end{pmatrix} \quad (2.12)$$

It can be observed that  $\bar{x}^+$  can be created as a function of  $x_k$  and  $\bar{u}$  using (2.8),

$$\bar{x}^+ = \begin{pmatrix} x_{k+1} \\ x_{k+2} \\ \vdots \\ x_{k+N} \end{pmatrix} = \begin{pmatrix} f(x_k, u_k) \\ f(x_{k+1}, u_{k+1}) \\ \vdots \\ f(x_{k+N-1}, u_{k+N-1}) \end{pmatrix} = \bar{f}(x_k, \bar{u}) \quad (2.13)$$

MPC solves an optimization problem in each iteration over the interval  $[k, k+N-1]$  using the current state ( $x_k$ ) as the initial state. Additionally, the optimization problem is subject to state-space model equation as the equality constraint and the limitations of the states and inputs as inequality constraints. The solution of the optimization problem is the control input sequence  $\bar{u}^*$ . The problem solution in each iteration can be formulated as [34] [35],

$$\begin{aligned} J^*(x_k, \bar{u}^*) = & \underset{\bar{u}}{\text{minimize}} && J(x_k, \bar{u}) \\ & \text{subject to} && \bar{x}^+ = \bar{f}(x_k, \bar{u}); \\ & && \bar{x} \in \mathcal{X}; \\ & && \bar{u} \in \mathcal{U}. \end{aligned} \quad (2.14)$$

where  $\mathcal{X}$  and  $\mathcal{U}$  are sets defined by the limitations of the states and inputs, respectively. The complete MPC algorithm is presented in Fig. 2.4.

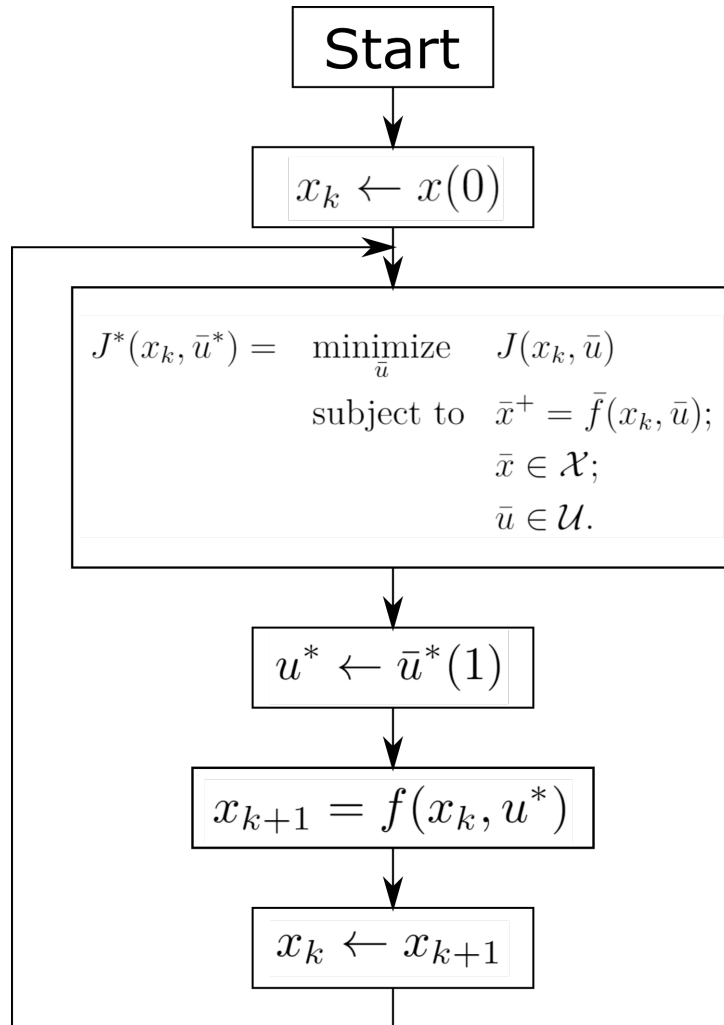


**Figure 2.4:** Model predictive control algorithm.

## 2. Background

---

# 3

## Modelling

The equality constraint of the optimization problem formulation in (2.14) contains the dynamics of system in its state-space representation. Changes or inaccuracies in the model will induce changes in the feasible set and, therefore, in the optimal solution obtained. Hence, a reliable system model is needed to obtain a reliable solution in each iteration of the MPC problem.

The Euler-Lagrange equation has been used to model different systems such as DC-DC power converters [36] [37], a robot manipulator [37], a quadrotor [38] and a one-legged robot [39] in previous studies. In contrast to classical mechanics, the Euler-Lagrange formalism decreases the complexity of the formulation when multi-body systems are under study. This is because the reaction forces are usually absent when the equations of motion are formulated [55].

Several studies using the Euler-Lagrange formalism to obtain the equations of motion of long combination vehicles (LCVs) has been published [40] [41] [42]. Also, other studies focused on semi-trailer combination have been done, see e.g. [43] and [44].

In this study the Euler-Lagrange equation is used to formulate the dynamics of the system. Studies done by H. B. Pacejka [45] and P. Nilsson *et al.* [46] are used as reference for modelling.

### 3.1 Road modeling

The Swedish Transport Administration regulates the design of the public roads in Sweden. For horizontal road geometry, three shapes are used for design: straight lines, circular arcs and clothoid segments [48]. Such a planar curve, formed by these three shapes, is called a clothoid spline [49] [50]. In order to create smooth curves, clothoid segments are always used as transitional curves between two straight lines, a straight line and a circular arc or two circular arcs of different radii [49] [22]. The curvature of each shape is described as [1],

$$c_h^{(i)}(s) = c_{h,0}^{(i)} + c_{h,1}^{(i)} \cdot s \quad (3.1)$$

### 3. Modelling

where  $s$  is the arc position,  $c_h^{(i)}$  is the curvature of each segment  $i$ ,  $c_{h,0}^{(i)}$  is the initial curvature and  $c_{h,1}^{(i)}$  is the curvature rate. Moreover,  $c_h^{(i)}$  is defined as,

$$c_h^{(i)} = \frac{d\psi_R^{(i)}(s)}{ds} \quad (3.2)$$

where  $\psi_R^{(i)}$  is the angle between the road tangent vector and the  $x$ -axis.

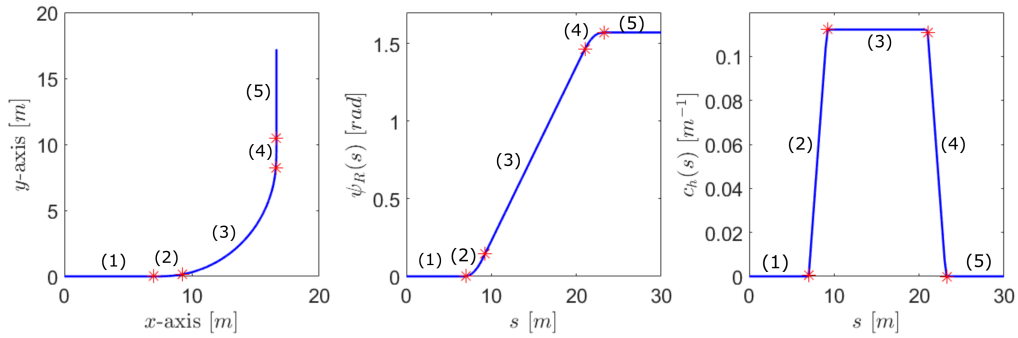


**Figure 3.1:** Road model parameters.

Fig. 3.1 shows a road segment represented as a clothoid spline (left) and the two parameter that describe the road:  $\psi_R$  (middle) and  $c_h$  (right). The road segment is divided in five parts: straight line (1), clothoid (2), circular arc (3), clothoid (4) and straight line (5). It is observed in Fig. 3.1 that the straight lines have zero curvature, whereas circular arcs have constant curvature different than zero. In the clothoid segments it is observed that the curvature is a linear function of  $s$ .

## 3.2 Vehicle motion modeling

### 3.2.1 System description

The vehicle combination consists of a  $6 \times 4$  tractor and a 3-axle semi-trailer as shown in Fig. 3.2. The characteristics of the semi-trailer used in this study follow the modular concept explained by J. Aurell *et al.* [51]. The model should be able to capture important motion characteristics and handle relevant driving scenarios. This is possible by using the two-track model presented in Fig. 3.3. However, by using this approach, a computationally demanding model is generated with many states and multiple inputs [1]. Gillespie *et al.* [52] published a linear analysis of the steady-state cornering performance of a multi-axle truck including the influence of dual tires and multiple non-steerable axles [53]. This model is based on a one-track model and it is presented in Fig. 3.4.

Figures 3.5, 3.6 and 3.7 show the one-track model of the vehicle combination and variables used in the model formulation of this study. Fig. 3.5 illustrates relevant dimensions, angles and coordinate frames. Fig. 3.6 illustrates position vectors of the center of masses, axles and connection point. Additionally, Fig. 3.7 illustrates motion variables and forces.

The notation, presented in Appendix A, is according to the ISO 8855 norm, [54], and P. Nilsson, [1].

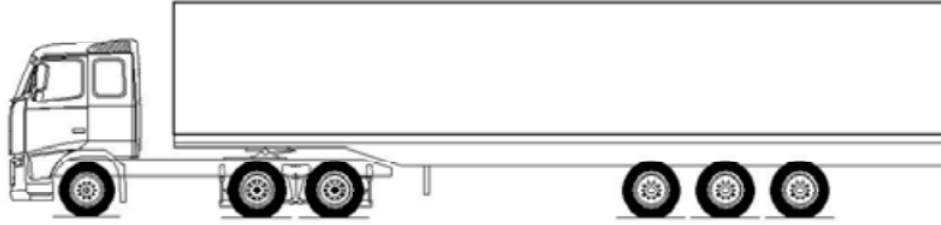


**Figure 3.2:** Semi-trailer combination [51].

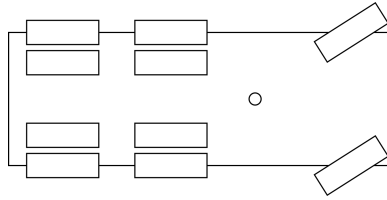


**Figure 3.3:** Two-track model with multiple non-steerable axles and dual tyres.

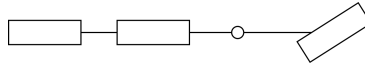


**Figure 3.4:** One-track model with multiple non-steerable axles and single tyres.

### 3.2.2 Rotation matrices

Fig. 3.5 shows four frames used in the modeling procedure,

$(X_E, Y_E)$	: Axis system fixed in the earth frame (Frame $\{E\}$ );
$(X_{W11}, Y_{W11})$	: Axis system fixed in unit 1 axle 1 (Frame $\{W\}$ );
$(X_{V1}, Y_{V1})$	: Axis system fixed in unit 1 (Frame $\{1\}$ );
$(X_{V2}, Y_{V2})$	: Axis system fixed in unit 2 (Frame $\{2\}$ ).

The following rotation matrices of frames  $\{W\}$ ,  $\{1\}$  and  $\{2\}$  with respect to frame  $\{E\}$  are calculated,

$$R_{v1} = R_z(\psi_1) = \begin{pmatrix} \cos \psi_1 & -\sin \psi_1 \\ \sin \psi_1 & \cos \psi_1 \end{pmatrix} \quad (3.3)$$

$$R_{v2} = R_z(\psi_2) = \begin{pmatrix} \cos \psi_2 & -\sin \psi_2 \\ \sin \psi_2 & \cos \psi_2 \end{pmatrix} = \begin{pmatrix} \cos(\psi_1 - \Delta\psi_1) & -\sin(\psi_1 - \Delta\psi_1) \\ \sin(\psi_1 - \Delta\psi_1) & \cos(\psi_1 - \Delta\psi_1) \end{pmatrix} \quad (3.4)$$

$$R_{w11} = R_z(\psi_1 + \delta_{11}) = \begin{pmatrix} \cos(\psi_1 + \delta_{11}) & -\sin(\psi_1 + \delta_{11}) \\ \sin(\psi_1 + \delta_{11}) & \cos(\psi_1 + \delta_{11}) \end{pmatrix} \quad (3.5)$$

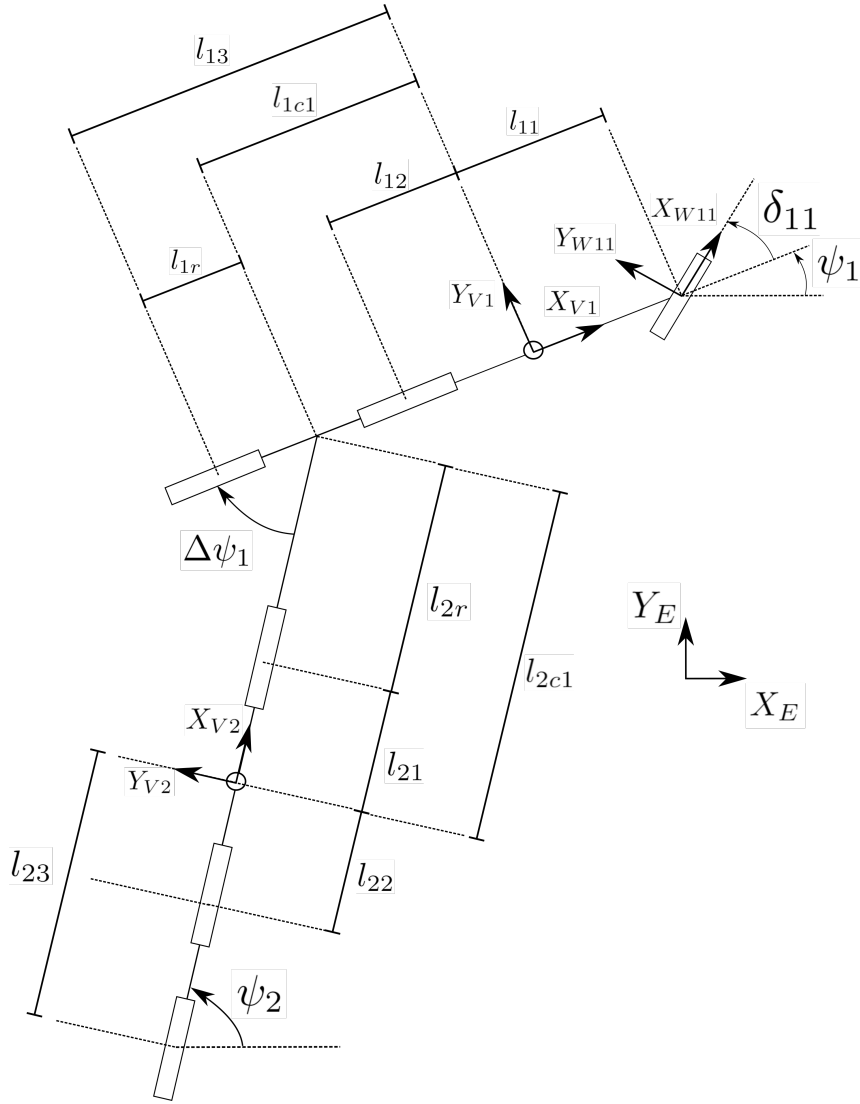


**Figure 3.5:** One-track model of a semi-trailer combination.

where,

- $R_{v1}$  : Rotation matrix for vehicle unit 1 (Frame  $\{1\}$ ) with respect to earth frame (Frame  $\{E\}$ );
- $R_{v2}$  : Rotation matrix for vehicle unit 2 (Frame  $\{2\}$ ) with respect to earth frame (Frame  $\{E\}$ );
- $R_{w11}$  : Rotation matrix for vehicle unit 1 axle 1 (Frame  $\{W\}$ ) with respect to earth frame (Frame  $\{E\}$ ).

### 3.2.3 Euler-Lagrange equation

The Euler-Lagrange equation is defined as [55],

$$\frac{d}{dt} \left( \frac{\partial \mathcal{L}(q, \dot{q})}{\partial \dot{q}} \right) - \frac{\partial \mathcal{L}(q, \dot{q})}{\partial q} = Q \quad (3.6)$$

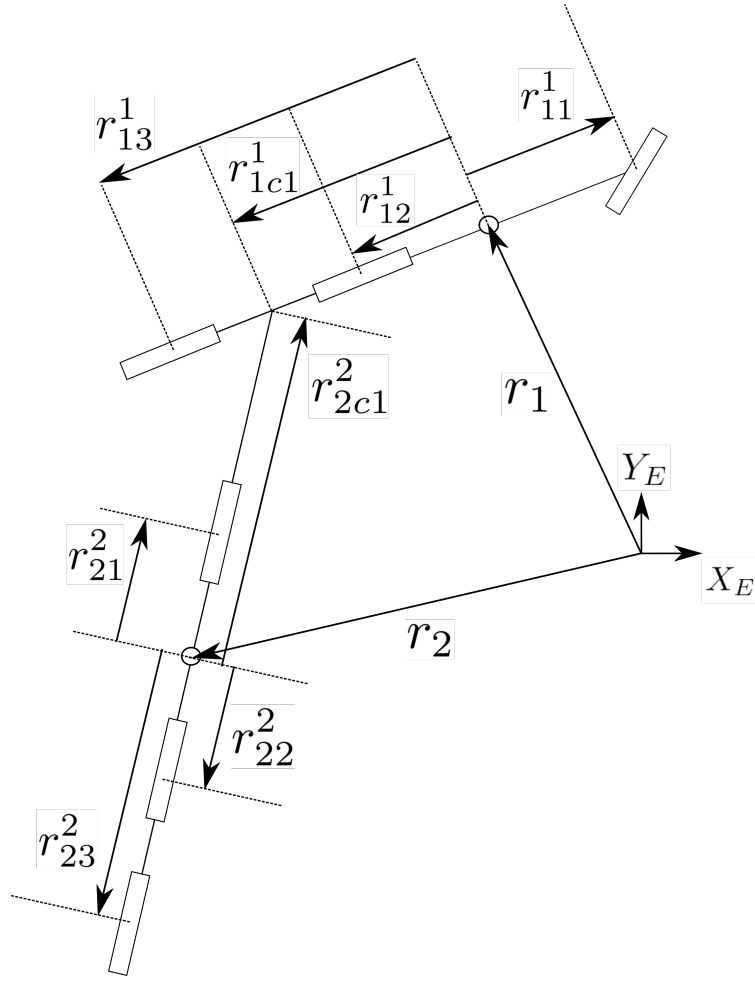


**Figure 3.6:** One-track model : Position vectors.

where  $q$  are the generalized coordinates,  $\mathcal{L}(q, \dot{q})$  is the Lagrangian for the system and  $Q$  are the generalized forces of the system. The Lagrangian is defined as,

$$\mathcal{L}(q, \dot{q}) = T(q, \dot{q}) - V(q) \quad (3.7)$$

where  $T(q, \dot{q})$  is the kinetic energy and  $V(q)$  is the potential energy. In this model it is considered a flat road. Therefore, the potential energy is neglected, i.e.  $V(q) = 0$ . Then, (3.6) can be expressed as,

$$\frac{d}{dt} \left( \frac{\partial T(q, \dot{q})}{\partial \dot{q}} \right) - \frac{\partial T(q, \dot{q})}{\partial q} = Q \quad (3.8)$$

By using the chain-rule, the following equivalent expression can be obtained,

$$\frac{d}{dt} \left( \frac{\partial T(q, \dot{q})}{\partial \dot{q}} \right) = \frac{\partial}{\partial q} \left( \frac{\partial T(q, \dot{q})}{\partial \dot{q}} \right) \frac{dq}{dt} + \frac{\partial}{\partial \dot{q}} \left( \frac{\partial T(q, \dot{q})}{\partial \dot{q}} \right) \frac{d\dot{q}}{dt} \quad (3.9)$$

$$\frac{d}{dt} \left( \frac{\partial T(q, \dot{q})}{\partial \dot{q}} \right) = \frac{\partial}{\partial q} \left( \frac{\partial T(q, \dot{q})}{\partial \dot{q}} \right) \dot{q} + \frac{\partial}{\partial \dot{q}} \left( \frac{\partial T(q, \dot{q})}{\partial \dot{q}} \right) \ddot{q} \quad (3.10)$$

Using (3.10) in (3.8), the Euler-Lagrange equation can be rewritten as,

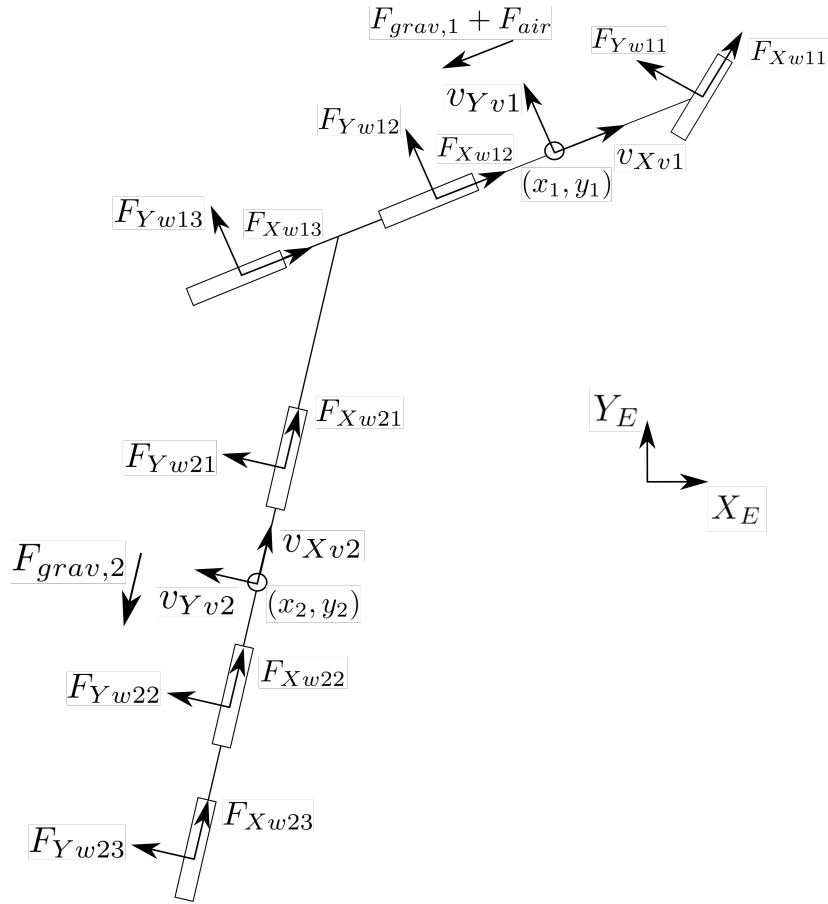


**Figure 3.7:** One-track model : Forces.

$$\frac{\partial}{\partial q} \left( \frac{\partial T(q, \dot{q})}{\partial \dot{q}} \right) \dot{q} + \frac{\partial}{\partial \dot{q}} \left( \frac{\partial T(q, \dot{q})}{\partial \dot{q}} \right) \ddot{q} - \frac{\partial T(q, \dot{q})}{\partial q} = Q \quad (3.11)$$

solving (3.11) for  $\ddot{q}$ ,

$$\ddot{q} = \left( \frac{\partial}{\partial \dot{q}} \left( \frac{\partial T(q, \dot{q})}{\partial \dot{q}} \right) \right)^{-1} \left( \frac{\partial T(q, \dot{q})}{\partial q} - \frac{\partial}{\partial q} \left( \frac{\partial T(q, \dot{q})}{\partial \dot{q}} \right) \dot{q} + Q \right) \quad (3.12)$$

The dynamics of the semi-trailer is described by the set of second order differential equations obtained in (3.12). In the following subsections,  $q$  is defined, and then,  $T(q, \dot{q})$  and  $Q$  are calculated in order to obtain the complete formulation of (3.12).

### 3.2.3.1 Generalized coordinates

The generalized coordinates of the system are defined as,

$$q = \begin{pmatrix} x_1 \\ y_1 \\ \psi_1 \\ \Delta\psi_1 \end{pmatrix} \longrightarrow \dot{q} = \begin{pmatrix} \dot{x}_1 \\ \dot{y}_1 \\ \dot{\psi}_1 \\ \Delta\dot{\psi}_1 \end{pmatrix} \longrightarrow \ddot{q} = \begin{pmatrix} \ddot{x}_1 \\ \ddot{y}_1 \\ \ddot{\psi}_1 \\ \Delta\ddot{\psi}_1 \end{pmatrix} \quad (3.13)$$

### 3.2.3.2 Kinetic energy

The total kinetic energy for the semi-trailer combination is given by,

$$T(q, \dot{q}) = \frac{1}{2}m_1v_1^T v_1 + \frac{1}{2}m_2v_2^T v_2 + \frac{1}{2}J_1\dot{\psi}_1^2 + \frac{1}{2}J_2\dot{\psi}_2^2 \quad (3.14)$$

where  $m_j$  are the masses of vehicle unit  $j$ ,  $v_j$  are the translational velocities vector for center of gravity of vehicle unit  $j$  and  $J_j$  are the moment of inertia about the  $z$ -axis. In order to calculate  $T(q, \dot{q})$ ;  $v_1$ ,  $v_2$  and  $\psi_2$  should be expressed as a function of  $q$  and  $\dot{q}$ .

From Figs. 3.5 and 3.6 is obtained,

$$r_{1c1}^1 = \begin{pmatrix} -l_{1c1} \\ 0 \end{pmatrix}, \quad r_{2c1}^2 = \begin{pmatrix} l_{2c1} \\ 0 \end{pmatrix} \quad (3.15)$$

Both vectors are represented in Frame  $\{1\}$ . In order to represent the same vectors with respect to Frame  $\{E\}$ , the following transformations are done, [56],

$$r_{1c1}^E = R_{v1} \begin{pmatrix} -l_{1c1} \\ 0 \end{pmatrix}, \quad r_{2c1}^E = R_{v2} \begin{pmatrix} l_{2c1} \\ 0 \end{pmatrix} \quad (3.16)$$

In Fig. 3.6 is observed that  $r_2$  can be calculated as,

$$r_2 = r_1 + r_{1c1}^E - r_{2c1}^E \quad (3.17)$$

$$r_2 = r_1 + R_{v1}r_{1c1}^1 - R_{v2}r_{2c1}^2 \quad (3.18)$$

Therefore, the position vectors of each center of gravity can be expressed as a function of  $q$ ,

$$r_1(q) = \begin{pmatrix} x_1 \\ y_1 \end{pmatrix} \quad (3.19)$$

$$r_2(q) = r_1 + R_{v1} \begin{pmatrix} -l_{1c1} \\ 0 \end{pmatrix} - R_{v2} \begin{pmatrix} l_{2c1} \\ 0 \end{pmatrix} \quad (3.20)$$

The translational velocities vector for center of gravity of vehicle unit  $j$  can be calculated as,

$$v_j(q, \dot{q}) = \dot{r}_j = \frac{\partial r_j}{\partial q} \dot{q}, \quad j \in \mathcal{N}_u \quad (3.21)$$

Furthermore, from Fig. 3.5,  $\psi_2$  can be determined as,

$$\psi_2(q) = \psi_1 - \Delta\psi_1 \quad (3.22)$$

### 3.2.3.3 Generalized forces

Fig. 3.7 shows the forces acting on the system. It is observed that those forces act on each axle and vehicle center of gravity. Then, the following general formulation can be used to calculate the generalized forces, [55] and [57]:

$$Q = \sum_{j \in \mathcal{N}_u} \sum_{k \in \mathcal{N}_a} \left( \frac{\partial r_{jk}}{\partial q} \right)^T F_{jk} + \sum_{j \in \mathcal{N}_u} \left( \frac{\partial r_j}{\partial q} \right)^T F_j \quad (3.23)$$

For the semi-trailer combination, the following expression is obtained using (3.23),

$$\begin{aligned}
 Q = & \left( \frac{\partial r_{11}}{\partial q} \right)^T F_{11} + \left( \frac{\partial r_{12}}{\partial q} \right)^T F_{12} + \left( \frac{\partial r_{13}}{\partial q} \right)^T F_{13} + \\
 & \left( \frac{\partial r_{21}}{\partial q} \right)^T F_{21} + \left( \frac{\partial r_{22}}{\partial q} \right)^T F_{22} + \left( \frac{\partial r_{23}}{\partial q} \right)^T F_{23} + \\
 & \left( \frac{\partial r_1}{\partial q} \right)^T F_1 + \left( \frac{\partial r_2}{\partial q} \right)^T F_2
 \end{aligned} \tag{3.24}$$

From Figs. 3.5 and 3.6, all the position vectors

$$\begin{aligned}
 r_{11}^1 &= \begin{pmatrix} l_{11} \\ 0 \end{pmatrix}, & r_{21}^2 &= \begin{pmatrix} l_{21} \\ 0 \end{pmatrix} \\
 r_{12}^1 &= \begin{pmatrix} -l_{12} \\ 0 \end{pmatrix}, & r_{22}^2 &= \begin{pmatrix} -l_{22} \\ 0 \end{pmatrix} \\
 r_{13}^1 &= \begin{pmatrix} -l_{13} \\ 0 \end{pmatrix}, & r_{23}^2 &= \begin{pmatrix} -l_{23} \\ 0 \end{pmatrix}
 \end{aligned} \tag{3.25}$$

are expressed with respect the fixed body frame of vehicle unit 1 and 2. In order to obtain the vector positions of each axle with respect to Frame  $\{E\}$ , the following transformations are needed [56],

$$\begin{pmatrix} r_{jk} \\ 1 \end{pmatrix} = H_j \begin{pmatrix} r_{jk}^j \\ 1 \end{pmatrix} = \begin{pmatrix} R_{vj} & r_j \\ 0_{1 \times 3} & 1 \end{pmatrix} \begin{pmatrix} r_{jk}^j \\ 1 \end{pmatrix} \tag{3.26}$$

where  $H_j$  is the homogeneous transformation matrix of Frame  $\{j\}$  with respect to Frame  $\{E\}$ . Then, the axles position vectors are calculated using,

$$r_{jk} = r_j + R_{vj} r_{jk}^j, \quad (j, k) \in \mathcal{N}_u \times \mathcal{N}_a \tag{3.27}$$

The translational velocity vector of vehicle unit  $j$  axle  $k$  with respect to the earth frame  $(v_{jk})$  can be define as,

$$v_{jk} = \frac{\partial r_{jk}}{\partial q} \dot{q} \tag{3.28}$$

This vector expressed in a wheel fixed frame can be calculated as,

$$\begin{pmatrix} v_{Xwjk} \\ v_{Ywjk} \end{pmatrix} = \begin{cases} R_{wjk} v_{jk} & , \quad (j, k) \in \{(1, 1)\} \\ R_{vj} v_{jk} & , \quad (j, k) \in \mathcal{N}_u \times \mathcal{N}_a - \{(1, 1)\} \end{cases} \tag{3.29}$$

Fig. 3.7 shows the forces acting on the semi-trailer combination. These forces are expressed in the fixed body frame of each unit and wheel. The forces acting on each center of mass are defined by,

$$F_{Xvj} = \begin{cases} F_{air} + F_{grav,j} & j = 1 \\ F_{grav,j} & j = 2 \end{cases} \tag{3.30}$$

$$F_{Yvj} = 0 \tag{3.31}$$

Assuming no longitudinal slip, small lateral slip and constant normal load, the lateral tyre forces can be approximated using, [45] and [47],

$$F_{Ywj k} = -C_{Yj k} \frac{v_{Ywj k}}{v_{Xwj k}} \quad (3.32)$$

where  $C_{Yj k}$  is the tyre cornering stiffness of unit  $j$  axle  $k$ .

The longitudinal tyre forces are generated by braking and propulsion and can be calculated as,

$$F_{Xwj k} = \begin{cases} F_{prop, j k} + F_{brake, j k} & , \quad (j, k) \in \{(1, 2)\} \\ 0 & , \quad \mathcal{N}_u \times \mathcal{N}_a - \{(1, 2)\} \end{cases} \quad (3.33)$$

In order to calculate  $F_j$  and  $F_{j k}$ , which are expressed with respect to Frame  $\{E\}$ , the force vectors  $(F_{xvj}, F_{yvj})$  and  $(F_{Xwj k}, F_{Ywj k})$  should be rotated,

$$F_j = R_{vj} \begin{pmatrix} F_{Xvj} \\ F_{Yvj} \end{pmatrix} \quad , \quad j \in \mathcal{N}_u \quad (3.34)$$

$$F_{j k} = \begin{cases} R_{wj k} \begin{pmatrix} F_{Xwj k} \\ F_{Ywj k} \end{pmatrix} & , \quad (j, k) \in \{(1, 1)\} \\ R_{vj} \begin{pmatrix} F_{Xwj k} \\ F_{Ywj k} \end{pmatrix} & , \quad (j, k) \in \mathcal{N}_u \times \mathcal{N}_a - \{(1, 1)\} \end{cases} \quad (3.35)$$

In this study the aerodynamic drag and gravitational forces are neglected. Therefore,

$$F_{Xvj} = F_{Yvj} = 0 \quad , \quad j \in \mathcal{N}_u \quad (3.36)$$

### 3.3 Vehicle motion in road coordinates

The position of any point in the earth frame can be expressed based on the road. In order to do this, two parameters are defined:  $s$  as the position along the road of the point projection on the road and  $d$  as the perpendicular distance from the road [22].

Fig. 3.8 shows the semi-trailer and road. In this study, the front and rearmost axle positions are described with respect to the the road as in previous studies done by P. Nilsson [1] and N.J. van Duijkeren [23]. The distances along the road for the unit 1 axle 1 and unit 2 axle 3 are represented by  $s_{R11}$  and  $s_{R23}$ , respectively. Moreover, the distances  $d_{R11}$  and  $d_{R23}$  correspond to the lateral distance offset perpendicular to the road for the unit 1 axle 1 and unit 2 axle 3, respectively.

The following expressions are obtained from P. Nilsson [1],

$$\dot{s}_{R11} = \frac{v_{Xv11} \cdot \cos(\psi_1 - \psi_R(s_{R11})) - v_{Yv11} \cdot \sin(\psi_1 - \psi_R(s_{R11}))}{1 - d_{R11} \cdot c_h(s_{R11})} \quad (3.37)$$

$$\dot{d}_{R11} = v_{Xv11} \cdot \sin(\psi_1 - \psi_R(s_{R11})) + v_{Yv11} \cdot \cos(\psi_1 - \psi_R(s_{R11})) \quad (3.38)$$

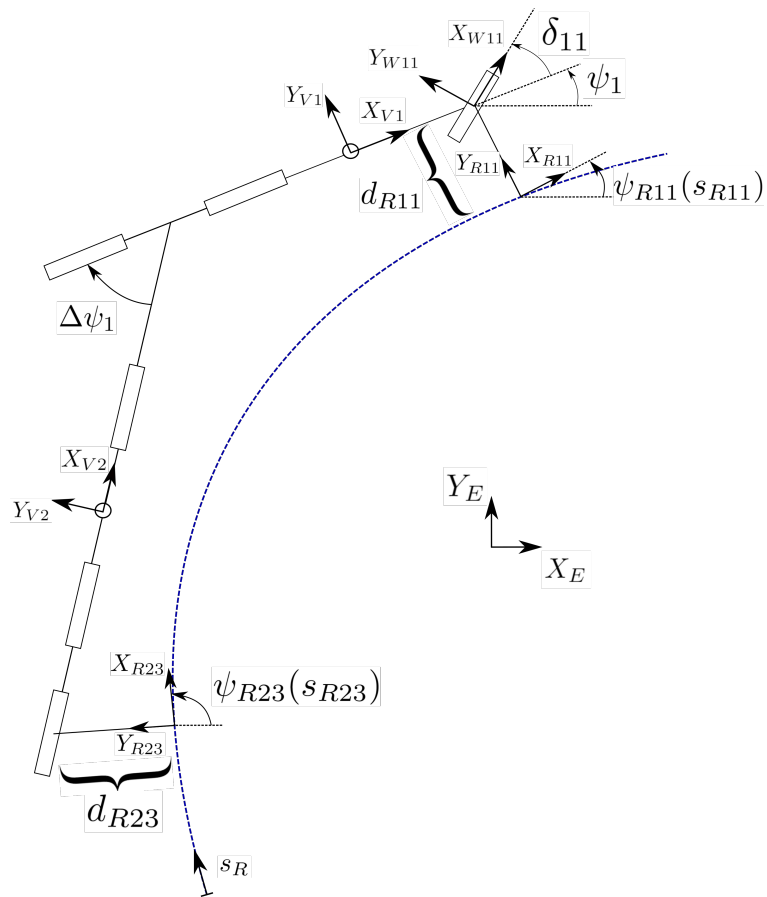
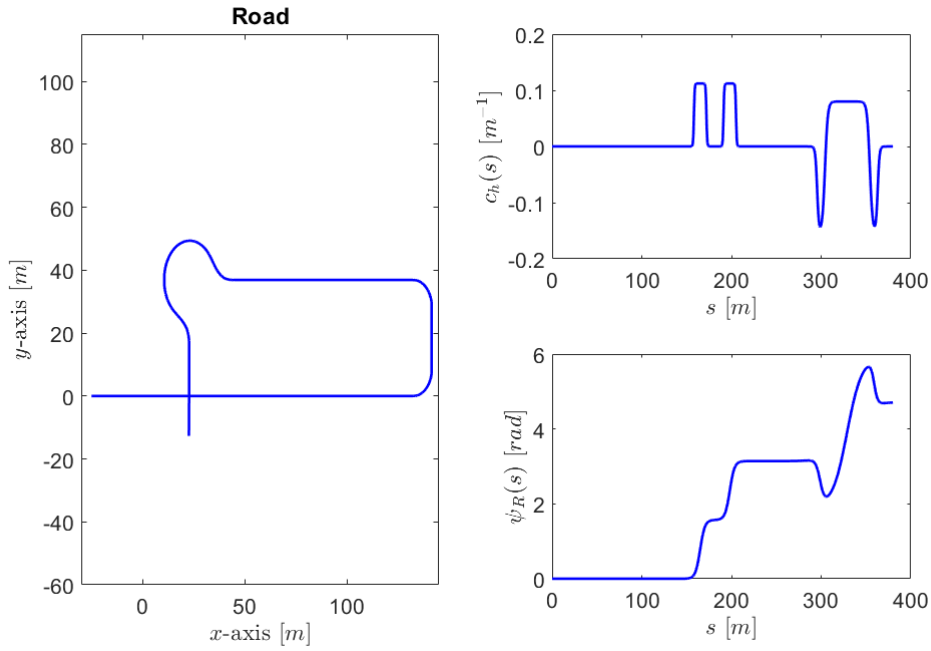


Figure 3.8: Semi-trailer motion relative to the road.



**Figure 3.9:** Road and its parameters.

$$\dot{s}_{R23} = \frac{v_{Xv23} \cdot \cos(\psi_2 - \psi_R(s_{R23})) - v_{Yv23} \cdot \sin(\psi_2 - \psi_R(s_{R23}))}{1 - d_{R23} \cdot c_h(s_{R23})} \quad (3.39)$$

$$\dot{d}_{R23} = v_{Xv23} \cdot \sin(\psi_2 - \psi_R(s_{R23})) + v_{Yv23} \cdot \cos(\psi_2 - \psi_R(s_{R23})) \quad (3.40)$$

where  $c_h$  is the curvature of the road segment  $\psi_R$  is the angle between the road tangent vector ( $X_{R11}$  or  $X_{R23}$ ) and the  $x$ -axis of the earth fixed frame ( $X_E$ ).

Fig. 3.9 shows the road used in this thesis and its parameters. In order to represent  $c_h$  and  $\psi_R$  as a function of  $s$ , a sigmoid function is used,

$$f_{\text{sigmoid}}(x) = \frac{A}{1 + e^{-m(x-x_c)}} \quad (3.41)$$

where parameters are defined as presented in Fig. 3.10. Then,  $c_h$  and  $\psi_R$  can be formulated as,

$$c_h(s) = \sum_j^N \frac{A_j}{1 + e^{-m_j(s-s_j)}} \quad (3.42)$$

$$\psi_R(s) = \sum_i^M \frac{A_i}{1 + e^{-m_i(s-s_i)}} \quad (3.43)$$

Fig. 3.11 shows the road segment represented in  $c_h$  and  $\psi_R$ .

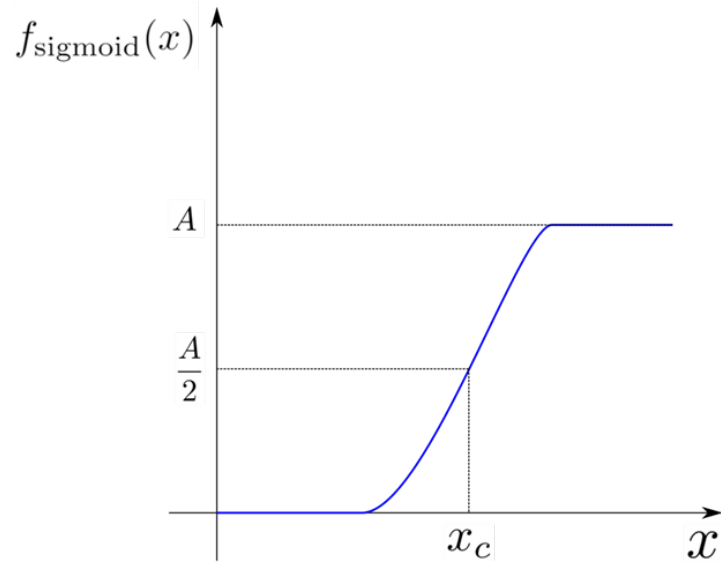


**Figure 3.10:** Sigmoid function.

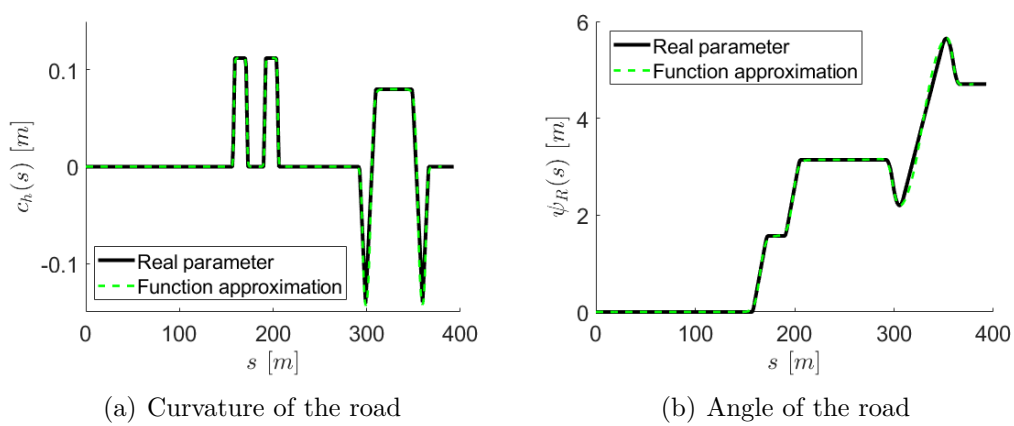


**Figure 3.11:** Road parameters approximation using sigmoid functions.

### 3.4 Nonlinear state-space model: Lateral and longitudinal dynamics

The following state and input vectors are selected for the semi-trailer nonlinear model,

$$X_{NL} = \begin{pmatrix} v_{x1} \\ v_{y1} \\ \psi_1 \\ \Delta\psi_1 \\ \psi_1 \\ \Delta\psi_1 \\ \delta_{11} \\ s_{R11} \\ d_{R11} \\ s_{R23} \\ d_{R23} \end{pmatrix}, \quad U_{NL} = \begin{pmatrix} \dot{\delta}_{11} \\ F_{Xw12} \end{pmatrix} \quad (3.44)$$

From (3.33), the longitudinal tyre force applied on unit 1 axle 2 is defined as,

$$F_{Xw12} = F_{prop,12} + F_{brake,12} \quad (3.45)$$

where  $F_{prop,12}$  and  $F_{brake,12}$  are the propulsion force and brake force in unit 1 axle 2 in the wheel fixed frame.

The nonlinear state-space model is defined by,

$$\dot{X}_{NL} = \begin{pmatrix} \dot{v}_{x1} \\ \dot{v}_{y1} \\ \dot{\psi}_1 \\ \dot{\Delta\psi}_1 \\ \dot{\psi}_1 \\ \dot{\Delta\psi}_1 \\ \dot{\delta}_{11} \\ \dot{s}_{R11} \\ \dot{d}_{R11} \\ \dot{s}_{R23} \\ \dot{d}_{R23} \end{pmatrix} = f_{NL}(X_{NL}, U_{NL}) \quad (3.46)$$

From (3.12) and (3.13), the following expressions are obtained as a function of  $q$  and  $\dot{q}$ ,

$$\ddot{q} = \begin{pmatrix} \ddot{x}_1 \\ \ddot{y}_1 \\ \ddot{\psi}_1 \\ \ddot{\Delta\psi}_1 \end{pmatrix} \quad (3.47)$$

In order to expressed the dynamics as a function of  $v_{Xv1}$  and  $v_{Yv1}$  instead of  $\dot{x}_1$  and  $\dot{y}_1$ , the following rotation is done,

$$\begin{pmatrix} \dot{x}_1 \\ \dot{y}_1 \end{pmatrix} = R_{v1} \begin{pmatrix} v_{Xv1} \\ v_{Yv1} \end{pmatrix} \quad (3.48)$$

Moreover, calculating the derivative with respect to time,

$$\begin{pmatrix} \ddot{x}_1 \\ \ddot{y}_1 \end{pmatrix} = \dot{R}_{v1} \begin{pmatrix} v_{Xv1} \\ v_{Yv1} \end{pmatrix} + R_{v1} \begin{pmatrix} \dot{v}_{Xv1} \\ \dot{v}_{Yv1} \end{pmatrix} \quad (3.49)$$

Rewriting (3.49),

$$\begin{pmatrix} \dot{v}_{Xv1} \\ \dot{v}_{Yv1} \end{pmatrix} = R_{v1}^T \left( \begin{pmatrix} \ddot{x}_1 \\ \ddot{y}_1 \end{pmatrix} - \dot{R}_{v1} \begin{pmatrix} v_{Xv1} \\ v_{Yv1} \end{pmatrix} \right) \quad (3.50)$$

The expressions from  $\ddot{x}_1$  and  $\ddot{y}_1$  are obtained from (3.12). These expressions are obtained as function of  $\dot{x}_1$ ,  $\dot{y}_1$ ,  $\psi_1$ ,  $\Delta\psi_1$ ,  $\dot{\psi}_1$  and  $\Delta\dot{\psi}_1$ . The expression (3.48) is used to expressed  $\dot{x}_1$  and  $\dot{y}_1$  as a function of  $v_{Xv1}$  and  $v_{Yv1}$ . Finally, (3.50) is used to obtain the expressions of  $\dot{v}_{Xv1}$  and  $\dot{v}_{Yv1}$  as a function of  $X_{NL}$ .

### 3.5 Nonlinear state-space model: Only lateral dynamics

A simplified nonlinear model is formulated assuming constant velocity of vehicle unit 1,

$$v_{Xv1} : \text{Constant} \quad (3.51)$$

i.e., it is assumed that all the longitudinal forces acting on this unit are zero.

$$F_{Xw11} \sin(\delta_{11}) + F_{Xw12} + F_{Xw13} = 0 \quad (3.52)$$

The coupling forces between unit 1 and 2 are neglected in order to simplify the calculation.

The following state vector and input are selected,

$$X_{nl} = \begin{pmatrix} v_{Yv1} \\ \dot{\psi}_1 \\ \Delta\psi_1 \\ \psi_1 \\ \Delta\dot{\psi}_1 \\ \delta_{11} \\ s_{R11} \\ d_{R11} \\ s_{R23} \\ d_{R23} \end{pmatrix}, \quad U_{nl} = \dot{\delta}_{11} \quad (3.53)$$

and the state-space model is defined by,

$$\dot{X}_{nl} = \begin{pmatrix} \dot{v}_{Yv1} \\ \ddot{\psi}_1 \\ \Delta\ddot{\psi}_1 \\ \dot{\psi}_1 \\ \Delta\dot{\psi}_1 \\ \dot{\delta}_{11} \\ \dot{s}_{R11} \\ \dot{d}_{R11} \\ \dot{s}_{R23} \\ \dot{d}_{R23} \end{pmatrix} = f_{nl}(X_{nl}, U_{nl}) \quad (3.54)$$

### 3.6 Linear model: Lateral and longitudinal dynamics

In this case the following nonlinear state-space model is defined.

$$\mathcal{X} = \begin{pmatrix} v_{Xv1} \\ v_{Yv1} \\ \dot{\psi}_1 \\ \Delta\dot{\psi}_1 \\ \psi_1 \\ \Delta\psi_1 \\ \delta_{11} \end{pmatrix}, \quad U = \begin{pmatrix} \dot{\delta}_{11} \\ F_{Xw12} \end{pmatrix} \rightarrow \dot{\mathcal{X}} = \begin{pmatrix} \dot{v}_{Xv1} \\ \dot{v}_{Yv1} \\ \ddot{\psi}_1 \\ \Delta\ddot{\psi}_1 \\ \dot{\psi}_1 \\ \Delta\dot{\psi}_1 \\ \dot{\delta}_{11} \end{pmatrix} = \mathcal{F}(\mathcal{X}, U) \quad (3.55)$$

The equilibrium point  $(\mathcal{X}_e, U_e)$  is selected as,

$$\mathcal{X}_e = \begin{pmatrix} v_{Xv1e} \\ v_{Yv1e} \\ \dot{\psi}_{1e} \\ \Delta\dot{\psi}_{1e} \\ \psi_{1e} \\ \Delta\psi_{1e} \\ \delta_{11e} \end{pmatrix} = \begin{pmatrix} v_{Xv1d} \\ 0 \\ 0 \\ 0 \\ 0 \\ 0 \\ 0 \end{pmatrix}, \quad U_e = \begin{pmatrix} \dot{\delta}_{11e} \\ F_{Xw12e} \end{pmatrix} = \begin{pmatrix} 0 \\ 0 \end{pmatrix} \quad (3.56)$$

where  $v_{Xv1d}$  is the desired longitudinal velocity of unit 1. Additionally, around the equilibrium point no acceleration is needed in order to keep constant longitudinal velocity. Therefore, the longitudinal force in unit 1 at the equilibrium point is defined as,

$$F_{Xw12e} = 0 \quad (3.57)$$

Then,  $\mathcal{F}$  can be linearized around the equilibrium point  $(\mathcal{X}_e, U_e)$  using (2.7),

$$\dot{\mathcal{X}} = A(v_{Xv1d})\mathcal{X} + B(v_{Xv1d})U \quad (3.58)$$

Using (3.58) in (3.46), a partial linear state-space equation is obtained,

$$\dot{X}_L = \begin{pmatrix} A(v_{Xv1d})\mathcal{X} + B(v_{Xv1d})U \\ \dot{s}_{R11} \\ \dot{d}_{R11} \\ \dot{s}_{R23} \\ \dot{d}_{R23} \end{pmatrix} = f_{LINEAR}(X_L, U_L) \quad (3.59)$$

where,

$$X_L = \begin{pmatrix} v_{x1} \\ v_{y1} \\ \psi_1 \\ \Delta\dot{\psi}_1 \\ \psi_1 \\ \Delta\psi_1 \\ \delta_{11} \\ s_{R11} \\ d_{R11} \\ s_{R23} \\ d_{R23} \end{pmatrix}, \quad U_L = \begin{pmatrix} \dot{\delta}_{11} \\ F_{Xw12} \end{pmatrix} \quad (3.60)$$

### 3.7 Linear model: Lateral dynamics

The following expressions are defined,

$$\mathcal{X} = \begin{pmatrix} v_{Yv1} \\ \dot{\psi}_1 \\ \Delta\dot{\psi}_1 \\ \psi_1 \\ \Delta\psi_1 \\ \delta_{11} \end{pmatrix} \longrightarrow \dot{\mathcal{X}} = \begin{pmatrix} \dot{v}_{Yv1} \\ \ddot{\psi}_1 \\ \Delta\ddot{\psi}_1 \\ \dot{\psi}_1 \\ \Delta\dot{\psi}_1 \\ \dot{\delta}_{11} \end{pmatrix} = \mathcal{F}(\mathcal{X}, U) \quad (3.61)$$

The equilibrium point  $(\mathcal{X}_e, U_e)$  is selected as,

$$\mathcal{X}_e = \begin{pmatrix} v_{Yv1e} \\ \psi_{1e} \\ \Delta\dot{\psi}_{1e} \\ \psi_{1e} \\ \Delta\psi_{1e} \\ \delta_{11e} \end{pmatrix} = \begin{pmatrix} 0 \\ 0 \\ 0 \\ 0 \\ 0 \\ 0 \end{pmatrix}, \quad U_e = \dot{\delta}_{11e} = 0 \quad (3.62)$$

Then,  $\mathcal{F}$  can be linearized around the equilibrium point using (2.7),

$$\dot{\mathcal{X}} = A(v_{Xv1})\mathcal{X} + B(v_{Xv1})U \quad (3.63)$$

where  $A$  and  $B$  are expressed as a function of  $v_{Xv1}$ . Using (3.63) in (3.54), a partial linear state-space equation is obtained,

$$\dot{X}_l = \begin{pmatrix} A(v_{Xv1})\mathcal{X} + B(v_{Xv1})U \\ \dot{s}_{R11} \\ \dot{d}_{R11} \\ \dot{s}_{R23} \\ \dot{d}_{R23} \end{pmatrix} = f_{\text{linear}}(X_l, U_l) \quad (3.64)$$

where,

$$X_l = \begin{pmatrix} v_{Xv1} \\ \dot{\psi}_1 \\ \Delta\psi_1 \\ \psi_1 \\ \Delta\psi_1 \\ \delta_{11} \\ s_{R11} \\ d_{R11} \\ s_{R23} \\ d_{R23} \end{pmatrix}, \quad U_l = \dot{\delta}_{11} \quad (3.65)$$

### 3.8 Kinematic model

The kinematic model approach neglects the lateral forces, mass and inertia of the vehicle [58] [24]. At low velocities, the tyre slip effects on the system can be neglected [59]. Therefore, since kinematic model neglects mass and inertia, this approach can give an accurate model if low velocity is used. Previous studies showed good performance of the kinematic model at low velocities [60] [61]. In this study, the methodology followed by Kalose [24] is used in order to obtain the kinematic model. The rearmost axle of the first unit, i.e. unit 1 axle 3, is chosen as the reference point. The position vector of the reference is defined as,

$$r_{13} = \begin{pmatrix} x_{13} \\ y_{13} \end{pmatrix} \quad (3.66)$$

A new set of generalized coordinates can be defined as,

$$q_{kin} = \begin{pmatrix} x_{13} \\ y_{13} \\ \psi_1 \\ \Delta\psi_1 \end{pmatrix} \longrightarrow \dot{q}_{kin} = \begin{pmatrix} \dot{x}_{13} \\ \dot{y}_{13} \\ \dot{\psi}_1 \\ \Delta\dot{\psi}_1 \end{pmatrix} \quad (3.67)$$

where,

$$\dot{x}_{13} = v_{Xv1} \cos(\psi_1) \quad (3.68)$$

$$\dot{y}_{13} = v_{Xv1} \sin(\psi_1) \quad (3.69)$$

The position vectors of the front and rearmost axles can be defined as,

$$r_{11} = r_{13} + R_{v1} \begin{pmatrix} L_{11} \\ 0 \end{pmatrix} \quad (3.70)$$

$$r_{23} = r_{1f} - R_{v2} \begin{pmatrix} L_{22} \\ 0 \end{pmatrix} \quad (3.71)$$

where,

$$r_{1f} = r_{13} + R_{v1} \begin{pmatrix} e_1 \\ 0 \end{pmatrix} \quad (3.72)$$

and  $L_{11}$  is the distance between the 2 axles of unit 1,  $L_{22}$  is the distance between the 2 axles of unit 2 and  $e_1$  is the distance between the rear axle of unit 1 and the joint point.

The velocity vectors can be calculated by,

$$v_{11} = \frac{\partial r_{11}}{\partial q_{kin}} \dot{q}_{kin} \quad (3.73)$$

$$v_{23} = \frac{\partial r_{23}}{\partial q_{kin}} \dot{q}_{kin} \quad (3.74)$$

In every axle, the lateral velocity should be zero. Therefore, the following constraint should hold,

$$\dot{y} \cos(\omega) - \dot{x} \sin(\omega) = 0 \quad (3.75)$$

where  $(\dot{x} \ \dot{y})^T$  is the velocity vector of the axle in the Frame  $\{E\}$ . Then, the following general expression is formulated,

$$\begin{cases} \hat{r}(\psi_j + \delta_{jk}) \cdot v_{jk} = 0 & , \quad (j, k) \in \{(1, 1)\} \\ \hat{r}(\psi_j) \cdot v_{jk} = 0 & , \quad (j, k) \in \mathcal{N}_u \times \mathcal{N}_a - \{(1, 1)\} \end{cases} \quad (3.76)$$

where  $\hat{r}(\omega)$  is a unit vector defined by,

$$\hat{r}(\omega) = \begin{pmatrix} -\cos(\omega) & \sin(\omega) \end{pmatrix} \quad (3.77)$$

This constraint is used in the front and rearmost axles,

$$\hat{r}(\psi_1 + \delta_{11}) \cdot v_{11} = 0 \quad (3.78)$$

$$\hat{r}(\psi_2) \cdot v_{23} = 0 \quad (3.79)$$

and solving (3.78) and (3.79) for  $\dot{\psi}_1$  and  $\Delta\dot{\psi}_1$  yields

$$\dot{\psi}_1 = \frac{\sin(\delta_{11})}{L_1 \cos(\delta_{11})} v_{Xv1} \quad (3.80)$$

$$\Delta\dot{\psi}_1 = \frac{L_2 \sin(\delta_{11}) - L_1 \cos(\delta_{11}) \sin(\Delta\psi_1) - L_{1r} \sin(\delta_{11}) \cos(\Delta\delta_{11})}{L_1 L_2 \cos(\delta_{11})} v_{Xv1} \quad (3.81)$$

where,

$$L_1 = l_{11} + l_{13} \quad (3.82)$$

$$L_2 = l_{23} + l_{2c1} \quad (3.83)$$

$$L_{1r} = l_{13} - l_{1c1} \quad (3.84)$$

Additionally, lateral velocity of unit 1 can be approximated by,

$$v_{Yv1} = l_{13}\dot{\psi}_1 \quad (3.85)$$

The following state and input vectors are defined,

$$X_{kin} = \begin{pmatrix} \psi_1 \\ \Delta\psi_1 \\ \delta_{11} \\ s_{R11} \\ d_{R11} \\ s_{R23} \\ d_{R23} \end{pmatrix}, \quad U_{kin} = \dot{\delta}_{11} \quad (3.86)$$

The kinematic state-space model can be formulated as,

$$\dot{X}_{kin} = \begin{pmatrix} \dot{\psi}_1 \\ \Delta\dot{\psi}_1 \\ \dot{\delta}_{11} \\ \dot{s}_{R11} \\ \dot{d}_{R11} \\ \dot{s}_{R23} \\ \dot{d}_{R23} \end{pmatrix} = f_{kin}(X_{kin}, U_{kin}) \quad (3.87)$$

### 3.9 Summary

Fig. 3.12 shows a summary of the modeling process. A nonlinear state-space model that describes the longitudinal and lateral dynamics of the semi-trailer is obtained ( $f_{NL}$ ) using the Euler-Lagrange formalism. A partial linear state-space model is obtained from  $f_{NL}$ . The dynamics of the semi-trailer are described by the first seven states of  $f_{NL}$ . These states are linearized around an equilibrium point ( $\mathcal{X}_e, U_e$ ) in order to obtain  $f_{LINEAR}$ .

If constant longitudinal velocity of unit 1 is assumed, the nonlinear state-space model can be expressed as  $f_{nl}$ . The lateral dynamics of the semi-trailer are described by the first six states of  $f_{nl}$ . These states are linearized around an equilibrium point ( $\mathcal{X}_e, U_e$ ) in order to obtain  $f_{linear}$ . Finally, the kinematic model approach is applied under these conditions. Using this approach  $\dot{\psi}_1$  and  $\Delta\dot{\psi}_1$  are estimated. Afterwards,  $f_{kin}$  is formulated.

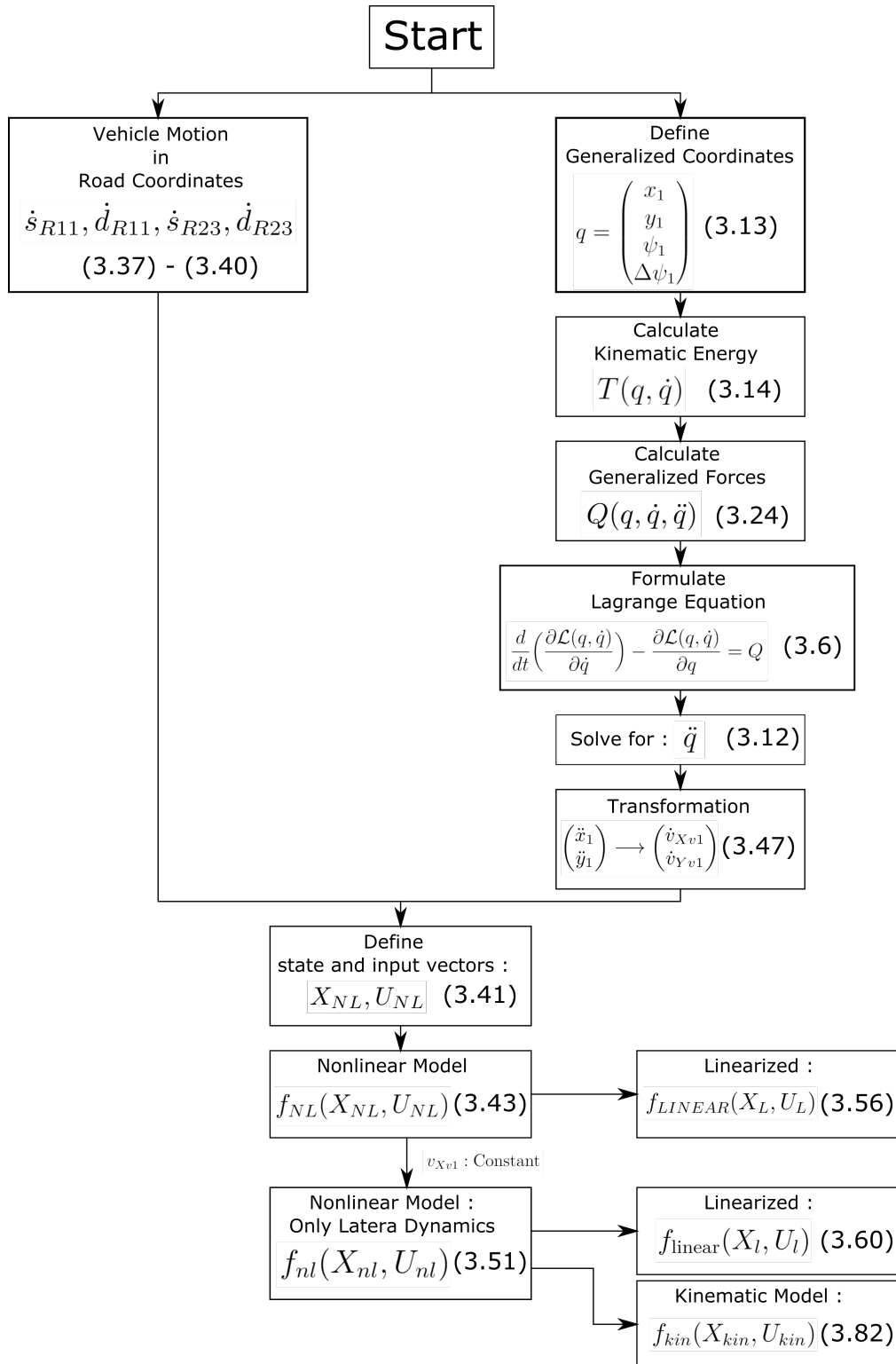


Figure 3.12: Modeling procedure summary.

# 4

## Proposed trajectory planning system

The aim of this study is road tracking considering physical limitations and safety of the vehicle combinations. In order to do this, two trajectory planners using MPC are formulated. Figures 4.1 and 4.2 show diagrams that include the trajectory planner, vehicle combination and controllers. In this study, the value of the vehicle combination state ( $X$ ) is known at any time instant and the characteristics of the road are known ( $\psi_R$  and  $c_h$ )

An optimization problem is formulated to be solved in every iteration of the MPC problem. The decision variable is defined as,

$$Z = \begin{pmatrix} \bar{u} \\ \bar{x} \end{pmatrix} \quad (4.1)$$

where  $\bar{u}$  and  $\bar{x}$  are defined in (2.10) and (2.11), respectively. Both vectors are constructed based on the state and input vectors selected for the state-space model of the system. After selecting the decision variable, a cost function, equality and inequality constraints should be defined as is presented in (2.14). The equality constraints are defined using the state-space equation of the model over the prediction horizon as shown in (2.13). The inequality constraints are selected based on the physical limitation of the system.

### 4.1 Longitudinal and lateral trajectory planner

The decision variable for the trajectory planner problem is built using  $X_L$  and  $U_L$ , which are defined in (3.60). Fig. 4.1 shows a diagram of the longitudinal and lateral trajectory planner in the system. For road tracking, two states of the system are minimized:  $d_{R11}$  and  $d_{R23}$ . The inputs are also penalized in this formulation. The steering angle rate ( $\dot{\delta}_{11}$ ) is minimized in order to achieve smooth behavior [22]. In order to achieve constant velocity in unit 1, the difference between  $v_{Xv1}$  and the reference velocity  $v_{Xv1}^{ref}$  is minimized. Finally,  $F_{Xw12}$  is minimized to avoid violent

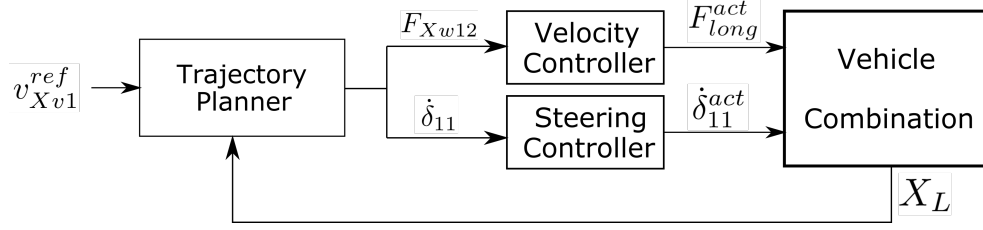


**Figure 4.1:** Diagram of the longitudinal and lateral trajectory planner in the system.

changes of velocity. Thus, the cost function to be minimized is formulated as,

$$\begin{aligned}
 J(Z) = & \sum_{i=k}^{k+N-1} \left( K_{\dot{\delta}_{11}} \cdot (\dot{\delta}_{11}(i))^2 + K_{F_{Xw12}} \cdot (F_{Xw12}(i))^2 \right. \\
 & + K_{v_{Xv1}} \cdot (v_{Xv1}(i) - v_{Xv1}^{ref})^2 \\
 & \left. + K_{d_{R11}} \cdot (d_{R11}(i))^2 + K_{d_{R23}} \cdot (d_{R23}(i))^2 \right)
 \end{aligned} \quad (4.2)$$

where  $K_{\dot{\delta}_{11}}$ ,  $K_{F_{Xw12}}$ ,  $K_{v_{Xv1}}$ ,  $K_{d_{R11}}$  and  $K_{d_{R23}}$  are tuning parameters used to penalize the contribution in the cost function of  $\dot{\delta}_{11}$ ,  $F_{Xw12}$ , the deviation of  $v_{Xv1}$  with respect to  $v_{Xv1}^{ref}$ ,  $d_{R11}$  and  $d_{R23}$ , respectively.

The cost function is minimized subject to constraints defined by the dynamics of the system and physical limitations in the states and inputs of the system. The equality constraints of the optimization problem includes the information of the dynamics of the system as shown in (2.13). The equality constraints are defined using  $f_{LINEAR}$  as state-space model. Additionally, in order to formulate the inequality constraints, boundaries in the states and inputs are defined based on physical limitations and safety,

$$\dot{\delta}_{11}^{min} \leq \dot{\delta}_{11} \leq \dot{\delta}_{11}^{max} \quad (4.3)$$

$$F_{Xw12}^{min} \leq F_{Xw12} \leq F_{Xw12}^{max} \quad (4.4)$$

$$\delta_{11}^{min} \leq \delta_{11} \leq \delta_{11}^{max} \quad (4.5)$$

$$d_{R11}^{min} \leq d_{R11} \leq d_{R11}^{max} \quad (4.6)$$

$$d_{R23}^{min} \leq d_{R23} \leq d_{R23}^{max} \quad (4.7)$$

$$v_{Xv1}^{min} \leq v_{Xv1} \leq v_{Xv1}^{max} \quad (4.8)$$

Bounds in  $d_{R11}$  and  $d_{R23}$  are defined in order to achieve road tracking, bounds in  $\delta_{11}$  for prevention of rolling over and bound in  $\dot{\delta}_{11}$  based on actuator limitations.

The complete optimization problem of the longitudinal and lateral trajectory planner ( $PLL_{linear}$ ) is formulated as,

$$\begin{aligned}
 J^*(x_k, \bar{u}^*) = \underset{\bar{u}}{\text{minimize}} \quad & \sum_{i=k}^{k+N-1} \left( K_{\dot{\delta}_{11}} \cdot (\dot{\delta}_{11}(i))^2 + K_{F_{Xw12}} \cdot (F_{Xw12}(i))^2 \right. \\
 & + K_{v_{Xv1}} \cdot (v_{Xv1}(i) - v_{Xv1}^{ref})^2 \\
 & \left. + K_{d_{R11}} \cdot (d_{R11}(i))^2 + K_{d_{R23}} \cdot (d_{R23}(i))^2 \right) \\
 \text{subject to} \quad & \bar{x}^+ = \bar{f}_{LINEAR}(x_k, \bar{u}); \\
 & d_{R11}^{min} \leq d_{R11} \leq d_{R11}^{max}; \\
 & d_{R23}^{min} \leq d_{R23} \leq d_{R23}^{max}; \\
 & \dot{\delta}_{11}^{min} \leq \dot{\delta}_{11} \leq \dot{\delta}_{11}^{max}; \\
 & \delta_{11}^{min} \leq \delta_{11} \leq \delta_{11}^{max}; \\
 & F_{Xw12}^{min} \leq F_{Xw12} \leq F_{Xw12}^{max}; \\
 & v_{Xv1}^{min} \leq v_{Xv1} \leq v_{Xv1}^{max}.
 \end{aligned} \tag{4.9}$$

The solution of the optimization problem ( $\bar{u}^*$ ) is an actuation trajectory in a horizon  $N$ .

## 4.2 Lateral trajectory planner

Fig. 4.2 shows a diagram of the lateral trajectory planner in the system. In this formulation, it is assumed constant velocity in unit 1. Therefore, only lateral dynamics are considered to formulate this problem.

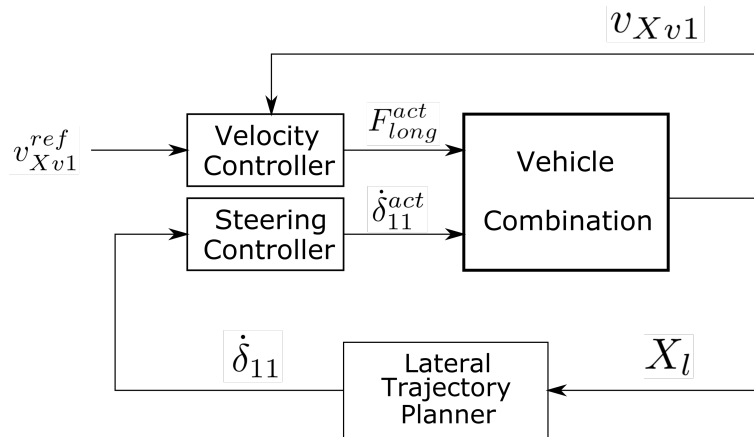


**Figure 4.2:** Diagram of the lateral trajectory planner in the system.

Two lateral trajectory planners are formulated in this study. The first one uses the partial linear state-space model defined in (3.64) to build the equality constraints. In this formulation,  $X_l$  and  $U_l$  are used as state and input vectors. The second one

#### 4. Proposed trajectory planning system

---

uses the kinematic model defined in (3.87) to build the equality constraints. In this case,  $X_{kin}$  and  $U_{kin}$  are used as state and input vectors.

The lateral trajectory planner using linear dynamics ( $PL_{linear}$ ) or the kinematic model ( $PL_{kinematic}$ ) can be formulated as,

$$\begin{aligned}
 J^*(x_k, \bar{u}^*) = \quad & \underset{\bar{u}}{\text{minimize}} && \sum_{i=k}^{k+N-1} \left( K_{\dot{\delta}_{11}} \cdot (\dot{\delta}_{11}(i))^2 \right. \\
 & && \left. + K_{d_{R11}} \cdot (d_{R11}(i))^2 + K_{d_{R23}} \cdot (d_{R23}(i))^2 \right) \\
 \text{subject to} & && \bar{x}^+ = \bar{f}_{lateral}(x_k, \bar{u}); \\
 & && d_{R11}^{min} \leq d_{R11} \leq d_{R11}^{max}; \\
 & && d_{R23}^{min} \leq d_{R23} \leq d_{R23}^{max}; \\
 & && \dot{\delta}_{11}^{min} \leq \dot{\delta}_{11} \leq \dot{\delta}_{11}^{max}; \\
 & && \delta_{11}^{min} \leq \delta_{11} \leq \delta_{11}^{max}.
 \end{aligned} \tag{4.10}$$

where  $\bar{f}_{lateral}$  can be  $\bar{f}_{linear}$  or  $\bar{f}_{kin}$ .

# 5

## Results

At the beginning of this chapter, the method to estimate the cornering stiffness values of the one truck model is presented. In order to estimate these parameters, different simulation tests are performed on the high-fidelity model. Then, simulation tests are implemented in order to validate and compare every simplified model (that was previously presented), with the high fidelity model.

Furthermore, each proposed trajectory planner is tested, using Forces Pro. During the simulations, the plant model that is used in every case is the corresponding dynamic/kinematic model used from the current trajectory planner.

In addition, the same simulation tests are performed using the high-fidelity model as a plant model. The results obtained from these tests can give to the reader a more realistic view of the performance of the proposed trajectory planners.

### 5.1 Cornering stiffness estimation

Tyre cornering stiffness value depends on several variables and tyre properties such as vertical load, steering angle, longitudinal velocity and slip angle [47]. In this study, the lateral tyre force is estimated using (3.32). Then, the cornering stiffness can be estimated by,

$$C_{Yjk} = -F_{Ywjk} \frac{v_{Xwjk}}{v_{Ywjk}} \quad (5.1)$$

where  $C_{Yjk}$  is the cornering stiffness of unit  $j$  axle  $k$ . The HF model provided by Volvo Trucks is used to estimate the cornering stiffness values,

$$C_{Yjk} = -F_{Ywjk}^m \frac{v_{Xwjk}^m}{v_{Ywjk}^m} \quad (5.2)$$

where  $F_{Ywjk}^m$ ,  $v_{Xwjk}^m$  and  $v_{Ywjk}^m$  are measured in the HF model. Simulations during 20 seconds with different  $v_{Xv1}$  and  $\delta_{11}$  values are performed. The sampling time of simulation is  $T_{simulation} = 0.001$  seconds. Values in the following interval are used,

$$v_{Xv1} \in [1.5, 5.5] \quad \text{m/s} \quad (5.3)$$

$$\delta_{11} \in [0.05, 0.5] \quad \text{rad} \quad (5.4)$$

Figures 5.1 and 5.2 show histograms of the estimations of each tyre. Finally, the cornering stiffness used for the one-track model with multiple axles is estimated by,

$$C_{Yjk} = C_{Yjk-left} + C_{Yjk-right} \quad (5.5)$$

Table 5.1 shows the cornering stiffness of each axle used in this model.

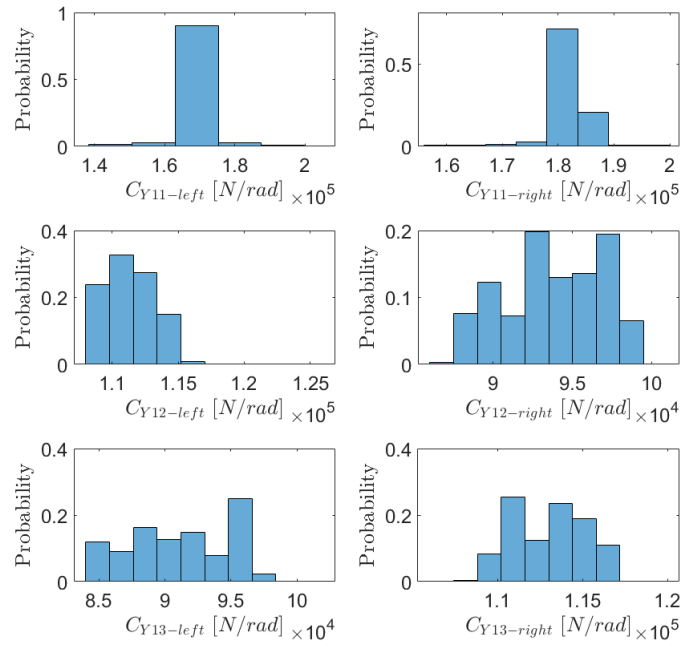


Figure 5.1: Cornering stiffness of unit 1.

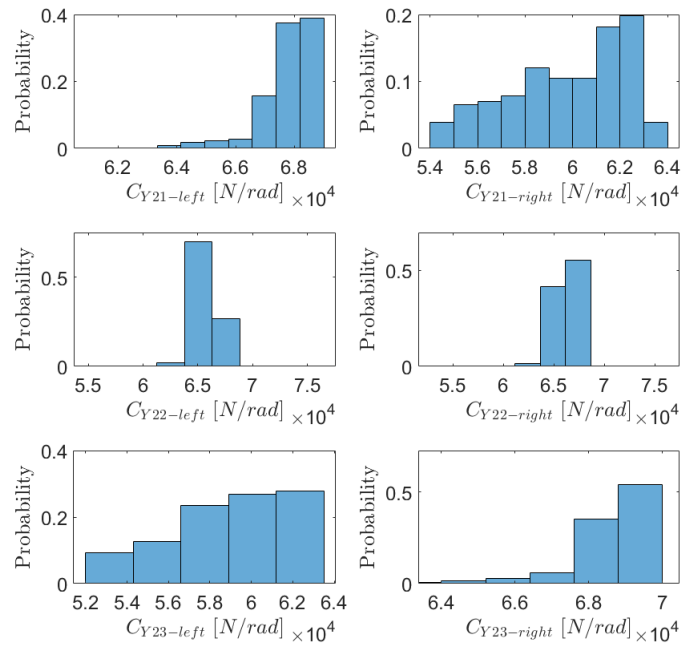


Figure 5.2: Cornering stiffness of unit 2.

Cornering Stiffness	Value
$C_{Y11}$	$35 \times 10^4$
$C_{Y12}$	$20 \times 10^4$
$C_{Y13}$	$20 \times 10^4$
$C_{Y21}$	$13 \times 10^4$
$C_{Y22}$	$13 \times 10^4$
$C_{Y23}$	$13 \times 10^4$

**Table 5.1:** Cornering stiffness estimated parameters.

## 5.2 Model validation

The high fidelity (HF) model is used to validate the nonlinear, linear and kinematic models obtained in this thesis. The HF model has two inputs: steering angle and acceleration request. In this study,  $F_{Xw12}$  is used instead of acceleration request since both values are linearly related,

$$F_{Xw12} = (m_1 + m_2)a_{req} \quad (5.6)$$

where  $a_{req}$  is the acceleration request.

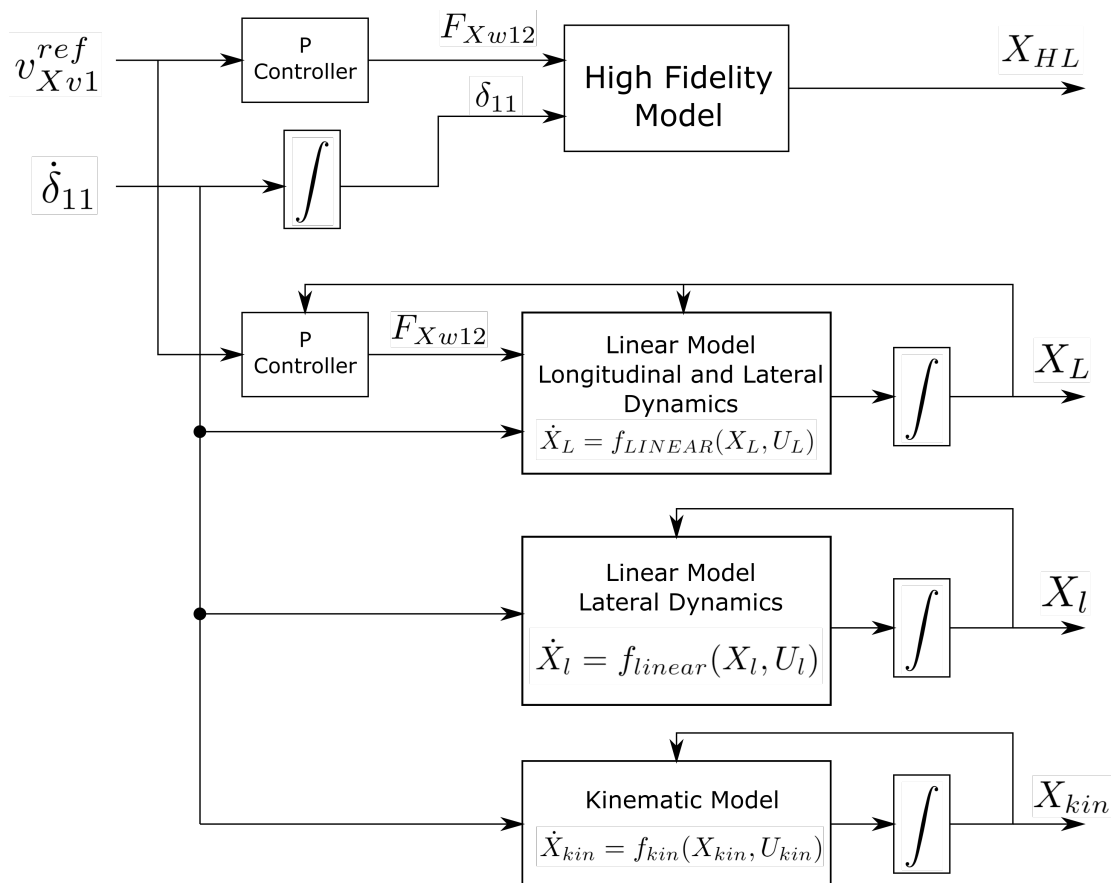


**Figure 5.3:** Model validation diagram.

Fig. 5.3 shows a diagram of the simulations performed to model validation. In order to compare the different models, constant velocity ( $v_{Xv1}^{ref}$ ) of vehicle unit 1 is used. To achieve this, a proportional controller is used in the HF model and  $f_{LINEAR}$  to keep  $v_{Xv1}$  constant. Moreover, the same input signal  $\dot{\delta}_{11}$  is used for all the models.

The error of the center of gravity estimation of vehicle unit  $j$  with respect to the HF model is calculated by,

$$e_{j-m}(t) = \left\| \begin{pmatrix} x_{j-HF}(t) \\ y_{j-HF}(t) \end{pmatrix} - \begin{pmatrix} x_{j-m}(t) \\ y_{j-m}(t) \end{pmatrix} \right\|_2 \quad (5.7)$$

where  $\begin{pmatrix} x_{j-HF}(t) & y_{j-HF}(t) \end{pmatrix}^T$  is the center of gravity of vehicle unit  $j$  calculated by the HF model and  $\begin{pmatrix} x_{j-m}(t) & y_{j-m}(t) \end{pmatrix}^T$  the center of gravity estimated by the model.

### 5.2.1 Model validation: Constant steering angle

In the first simulation, a constant steering angle of  $\delta_{11} = 5^\circ$  is used. In order to achieve this, the following input and initial conditions are considered,

$$\dot{\delta}_{11}(t) = 0 \quad (5.8)$$

$$\delta_{110} = 5^\circ \quad (5.9)$$

where  $\delta_{110}$  is the initial condition of  $\delta_{11}$ . The following condition are considered,

$$v_{Xv1}^{ref} = 2.5 \text{ m/s} \quad (5.10)$$

$$T_{simulation} = 10 \text{ s} \quad (5.11)$$

Fig. 5.4 shows the estimated center of gravity of unit 1 and 2 using the different models. Fig. 5.5 shows the estimation error calculated using (5.7). Fig. 5.6 shows the estimation of  $\psi_1$  and  $\Delta\psi_1$ . The dashed black lines are the results from the HF model. The blue lines are the estimations using the linear model of lateral and longitudinal dynamics ( $f_{LINEAR}$ ). The dashed green lines are the estimation using the linear model of lateral dynamics  $f_{linear}$ . The red lines are the estimations using the kinematic model ( $f_{kin}$ ).

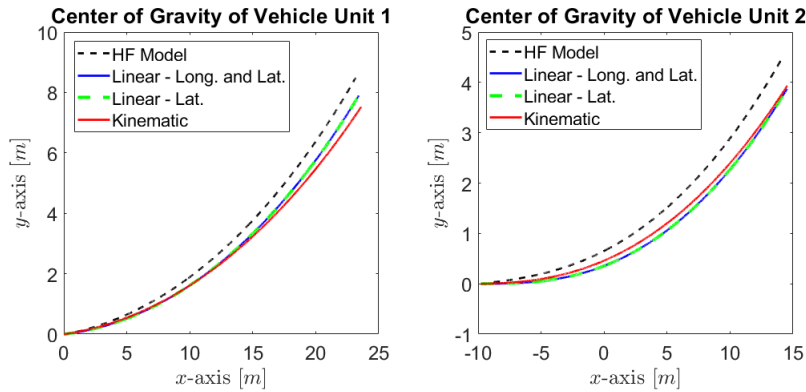


**Figure 5.4:** Center of gravity of vehicle unit 1 and 2. Input  $\dot{\delta}_{11}(t) = 0$  and initial condition  $\delta_{110} = 5^\circ$ .

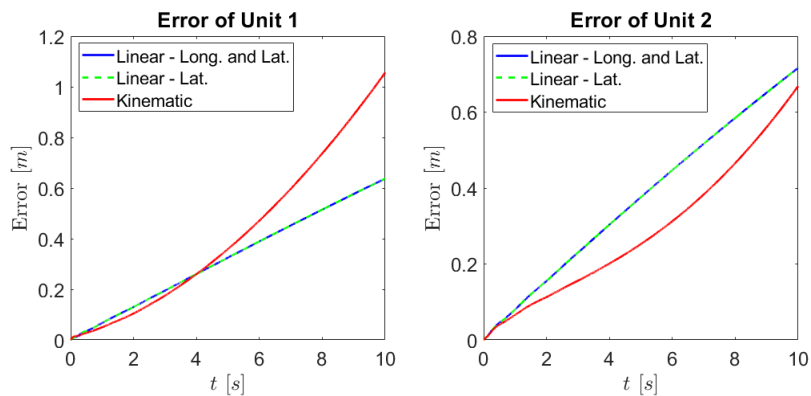


**Figure 5.5:** Error estimation of the center of gravity of vehicle unit 1 and 2 by the nonlinear and linear mode. Input  $\dot{\delta}_{11}(t) = 0$  and initial condition  $\delta_{110} = 5^\circ$ .

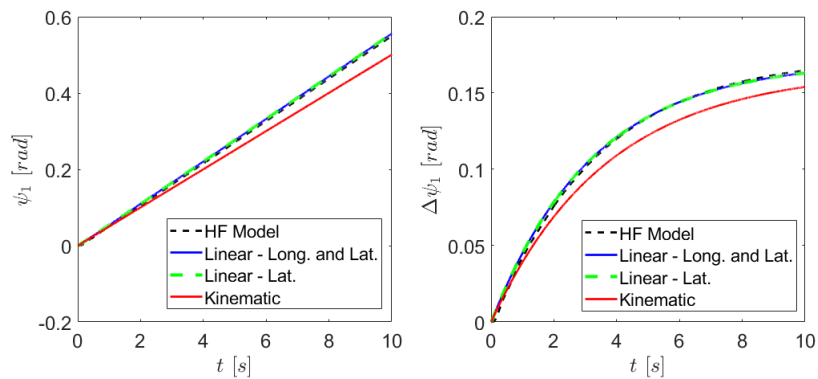


**Figure 5.6:** Estimation of  $\psi_1$  and  $\Delta\psi_1$ . Input  $\dot{\delta}_{11}(t) = 0$  and initial condition  $\delta_{110} = 5^\circ$ .

### 5.2.2 Model validation: Sinusoidal steering angle

In the second test, uses the following input to the three models,

$$\dot{\delta}_{11}(t) = A \cdot \cos 2\pi \cdot f \cdot t \quad (5.12)$$

where  $A = 0.1053 \text{ rad/s}$  and  $f = 0.08 \text{ Hz}$ . Moreover, constant longitudinal velocity of vehicle unit 1 is considered,

$$v_{Xv1}^{ref} = 2.5 \text{ m/s} \quad (5.13)$$

The simulation time is  $T_{simulation} = 20 \text{ s}$  and the results are shown in Figures 5.7, 5.8 and 5.9.

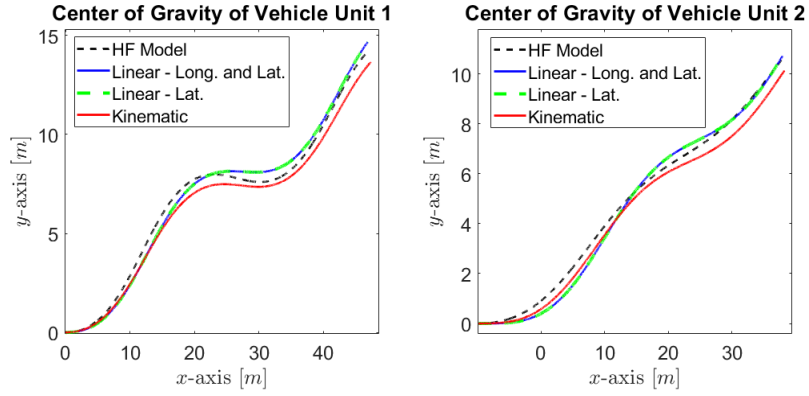


**Figure 5.7:** Center of gravity of vehicle unit 1 and 2. Input  $\dot{\delta}_{11}(t) = A \cdot \cos 2\pi \cdot f \cdot t$  and initial condition  $\delta_{110} = 0^\circ$ .  $A = 0.1053 \text{ rad/s}$  and  $f = 0.08 \text{ Hz}$ .

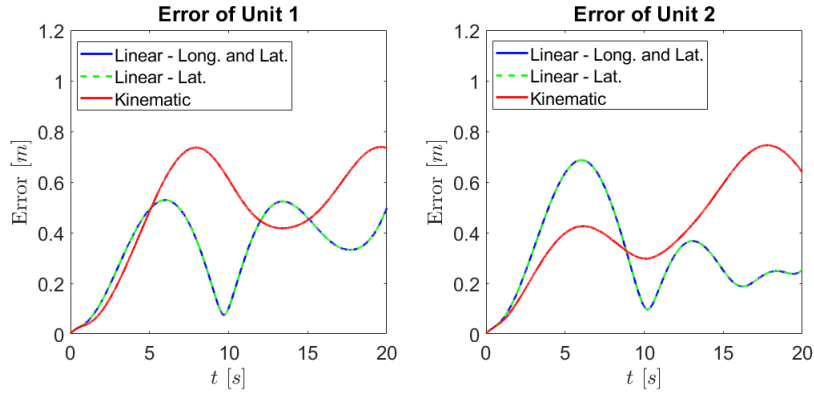


**Figure 5.8:** Error estimation of the center of gravity of vehicle unit 1 and 2 by the nonlinear and linear mode. Input  $\dot{\delta}_{11}(t) = A \cdot \cos 2\pi \cdot f \cdot t$  and initial condition  $\delta_{110} = 0^\circ$ .  $A = 0.1053 \text{ rad/s}$  and  $f = 0.08 \text{ Hz}$ .

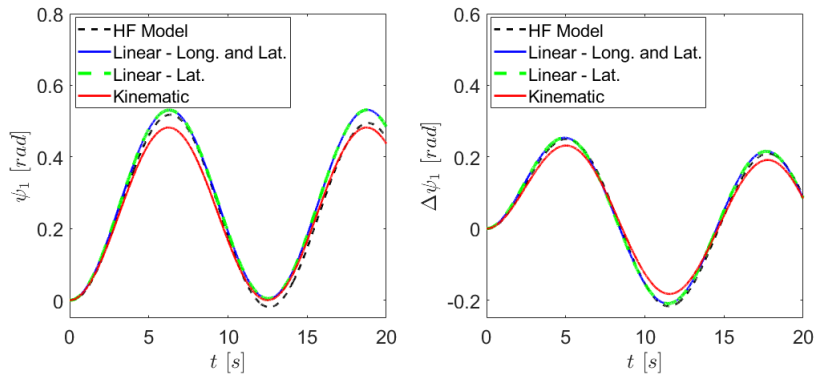


**Figure 5.9:** Estimation of  $\psi_1$  and  $\Delta\psi_1$ . Input  $\dot{\delta}_{11}(t) = A \cdot \cos 2\pi \cdot f \cdot t$  and initial condition  $\delta_{110} = 0^\circ$ .  $A = 0.1053 \text{ rad/s}$  and  $f = 0.08 \text{ Hz}$ .

### 5.3 Trajectory planner: Simulations using Forces Pro solver and nonlinear state-space model

The discrete state-space models ( $f_{LINEAR}$ ,  $f_{linear}$  or  $f_{kin}$ ) used as equality constraints are obtained using the Forward-Euler method with a sampling time  $T_s$ . The state sequence, input sequence and the next step state sequence are formulated using steps intervals of  $T_\Delta$  seconds. The prediction horizon ( $T_{horizon}$ ) of the MPC problem is selected as,

$$T_{horizon} = 8 \quad s \quad (5.14)$$

The following equation is used to calculate the number of samples of horizon,

$$N = \frac{T_{horizon}}{T_\Delta} \quad (5.15)$$

The  $T_s$  and  $T_\Delta$  values selected for the different planners are presented in Table 5.2. Finally, the following longitudinal velocity reference of unit 1 is selected,

$$v_{Xv1}^{ref} = 3 \quad \text{m/s} \quad (5.16)$$

The lateral trajectory planners ( $PL_{linear}$  and  $PL_{kinematic}$ ) boundaries and tuning parameters are presented in Table 5.3. Moreover, the nonlinear state-space  $f_{NL}$  is used for the simulations.

Trajectory Planner	$T_s$ [s]	$T_\Delta$ [s]
$PLL_{linear}$	0.01	0.25
$PL_{linear}$	0.01	0.25
$PL_{kinematic}$	0.02	0.25

**Table 5.2:** Values of  $T_s$  and  $T_\Delta$  for each planner.

Constant	Value
$K_{\dot{\delta}_{11}}$	10
$K_{d_{R11}}$	30
$K_{d_{R23}}$	80
$d_{R11}^{min}$	-3.5
$d_{R11}^{max}$	+3.5
$d_{R23}^{min}$	+2.5
$d_{R23}^{max}$	+2.5
$\delta_{11}^{min}$	-0.2
$\delta_{11}^{max}$	+0.2
$\delta_{11}^{min}$	-0.4
$\delta_{11}^{max}$	+0.4

**Table 5.3:** Lateral trajectory planners: Tuning parameters and boundaries.

The longitudinal and lateral trajectory planner ( $PLL_{linear}$ ) is designed using the formulation in (4.9). The diagram of the simulation is presented in Fig. 4.1. In this formulation, the acceleration constraint of vehicle unit 1 is defined by,

$$\left| a_{Xv1} \right| \leq a_{Xv1}^{lim} \quad (5.17)$$

The following relationship can be considered around the stationary point used to obtain the linear models,

$$F_{Xw12} = (m_1 + m_2) \cdot a_{Xv1} \quad (5.18)$$

The boundaries for  $F_{Xw12}$  are defined by

$$\left| F_{Xw12} \right| \leq (m_1 + m_2) \cdot a_{Xv1}^{lim} \quad (5.19)$$

The following acceleration limit is considered in this study,

$$a_{Xv1}^{lim} = 2 \quad m/s^2 \quad (5.20)$$

Table 5.4 shows the boundaries and tuning parameters. Fig. 5.10 shows the road tracking results. Fig. 5.11 shows the optimal control input obtained by the planners ( $\delta_{11}$ ) and  $\delta_{11}$ . It is observed that the three planners have similar results. Similar  $d_{R11}$ ,  $d_{R23}$  and  $\delta_{11}$  values are obtained. However, some differences in the optimization problem solving time is observed in Fig. 5.12.  $PL_{kinematic}$  is the fastest planner. It has a mean solving time of 0.015 seconds, while  $PL_{linear}$  planner has a mean solving time of 0.028 seconds and  $PLL_{linear}$  a mean solving time value of 0.032 seconds.

Constant	Value
$K_{\dot{\delta}_{11}}$	200
$K_{F_{Xw12}}$	0.00002
$K_{v_{Xv1}}$	500
$K_{d_{R11}}$	1
$K_{d_{R23}}$	10
$d_{R11}^{min}$	-3.5
$d_{R11}^{max}$	+3.5
$d_{R23}^{min}$	+2.5
$d_{R23}^{max}$	+2.5
$\delta_{11}^{min}$	-0.2
$\delta_{11}^{max}$	+0.2
$\delta_{11}^{min}$	-0.4
$\delta_{11}^{max}$	+0.4
$F_{Xw12}^{min}$	-39482
$F_{Xw12}^{max}$	+39482
$v_{Xv1}^{min}$	1.5
$v_{Xv1}^{max}$	3.5

**Table 5.4:** Trajectory planner using linear longitudinal and lateral dynamics model: Tuning parameters and boundaries.

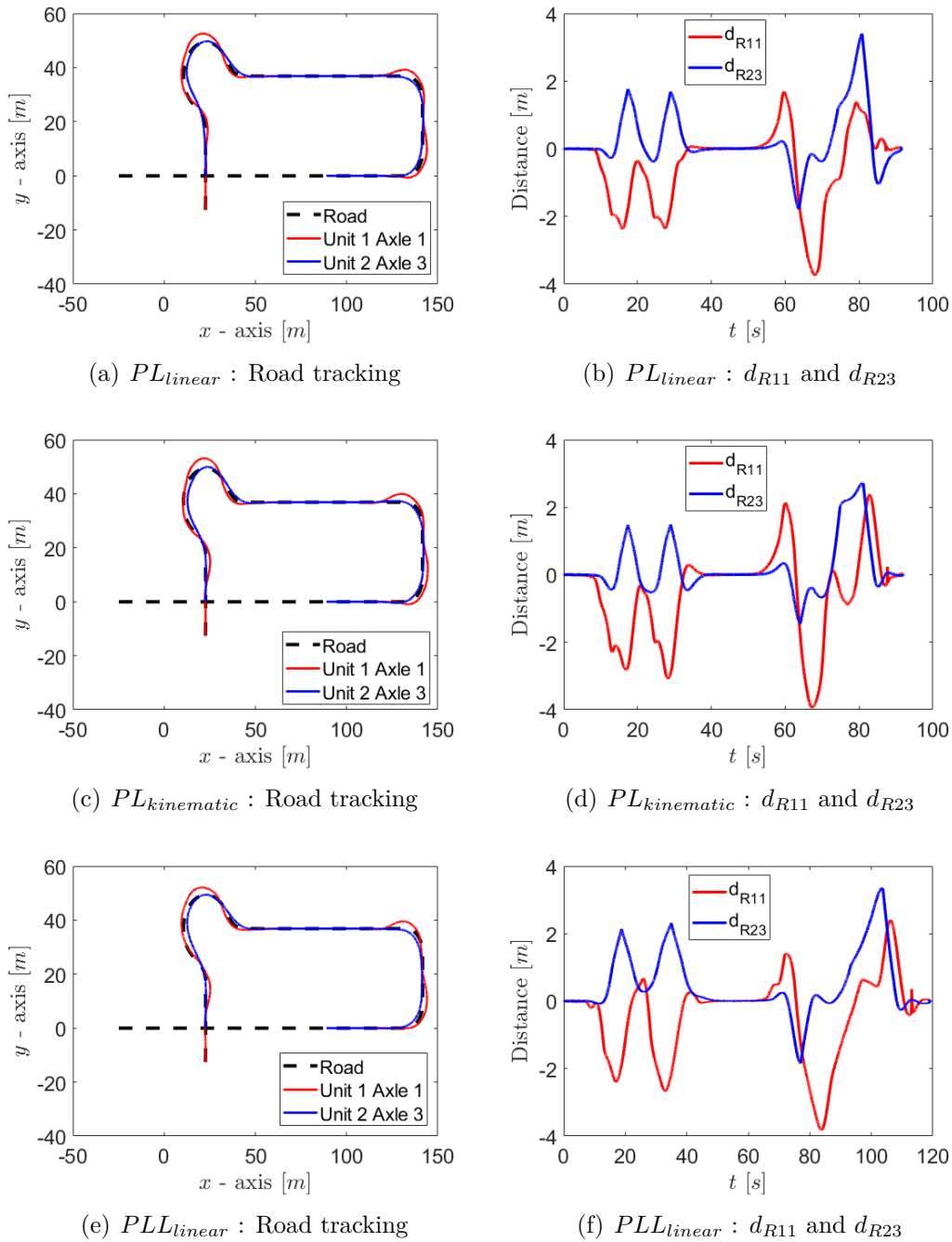


**Figure 5.10:** Simulations using nonlinear model and Forces Pro solver: Road tracking,  $d_{R11}$  and  $d_{R23}$ .

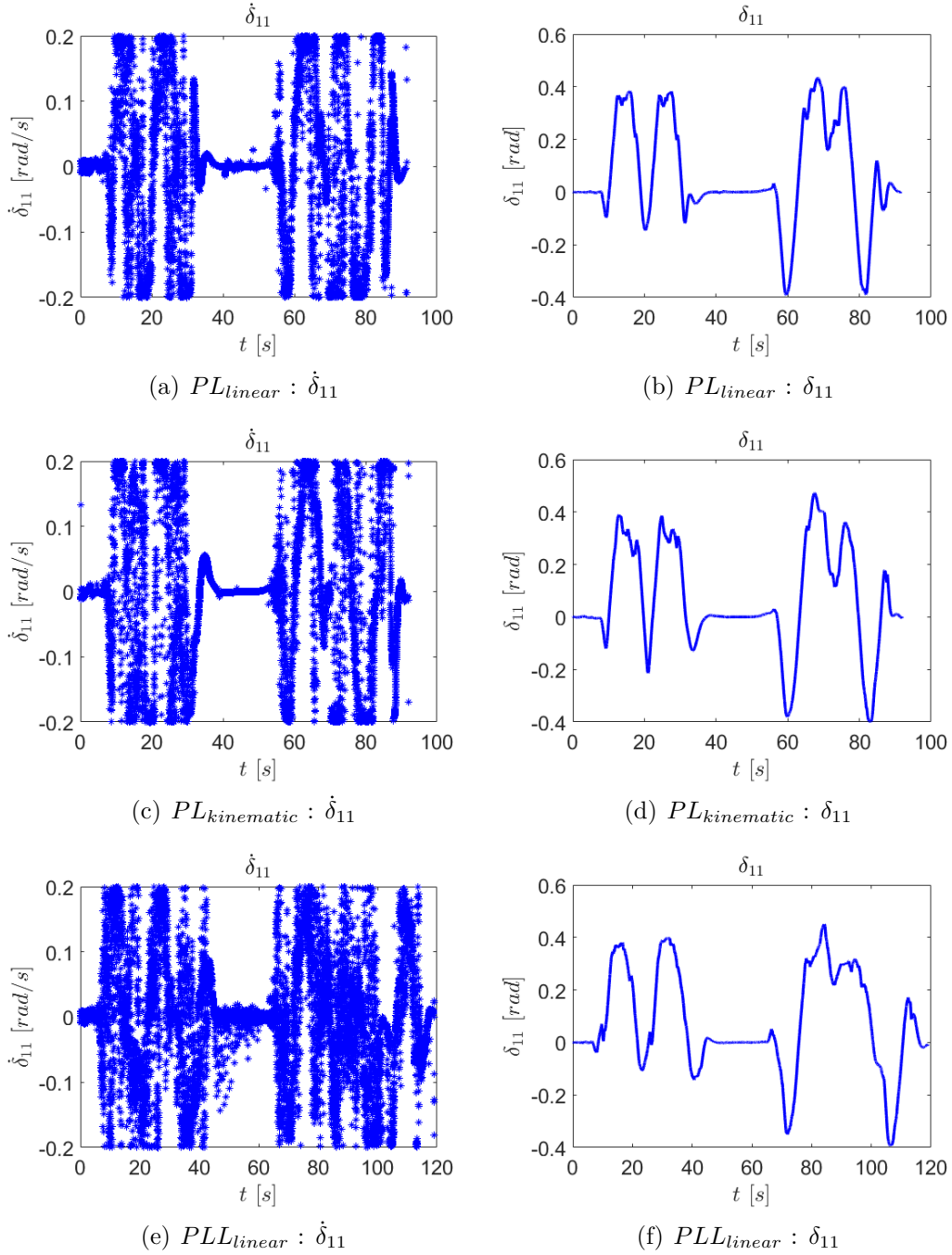


**Figure 5.11:** Simulations using nonlinear model and Forces Pro solver:  $\delta_{11}$  and  $\dot{\delta}_{11}$ .

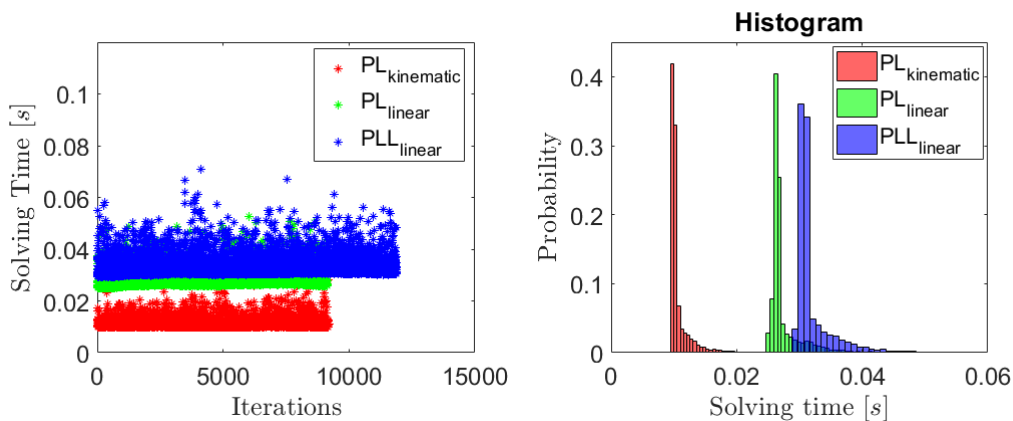
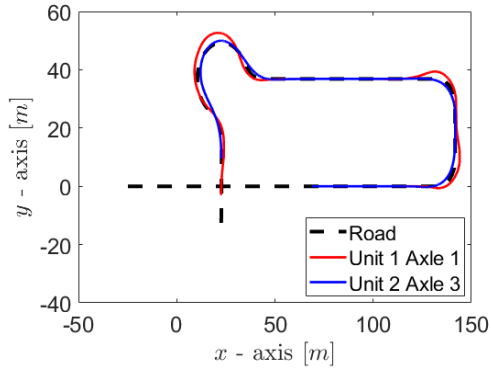


**Figure 5.12:** Simulation using nonlinear model and Forces Pro: Planner solving time.

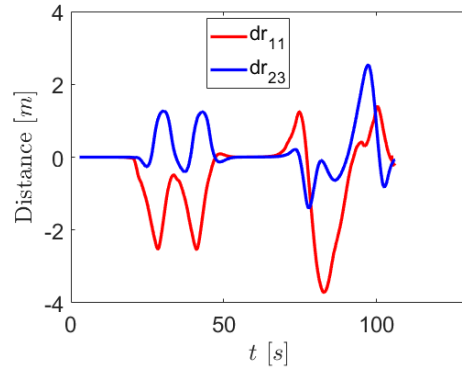
## 5.4 Trajectory planner: Real time simulations using Forces Pro solver and HF model

The trajectory planners are tested using the HF model provided by Volvo Trucks. Real time simulations using ROS are performed. The frequency publish ROS topic is set to 20 hz.

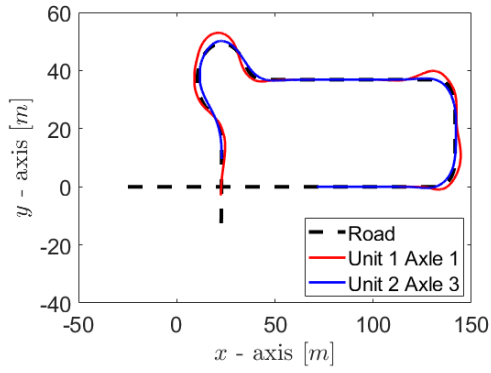
The same tuning parameters are used in this simulation (Table 5.4). Fig. 5.13 shows the road tracking results. Fig. 5.14 shows the optimal control input obtained by the planners ( $\delta_{11}^*$ ) and  $\delta_{11}$ . As in the previous simulations, the three planners have similar results for the optimal control input and states. In simulations using  $PL_{linear}$  and  $PL_{kinematic}$ , an additional longitudinal controller is used. On the other hand,  $PLL_{linear}$  planner includes lateral and longitudinal predictions. Fig. 5.15 shows  $v_{Xv1}$  values during simulations. Finally,  $PL_{kinematic}$  is the fastest planner as well. The optimization problem solving time is presented in Fig. 5.16. In this case,  $PL_{kinematic}$  has a mean solving time of 0.012 , while  $PL_{linear}$  planner has a mean solving time of 0.032 seconds and  $PLL_{linear}$  a mean solving time value of 0.039 seconds. It is observed that the standard deviation of the solving time is higher than in simulations using the nonlinear state-space model.



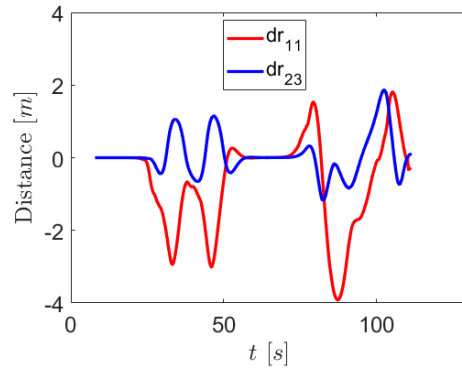
(a)  $PL_{linear}$  : Road tracking



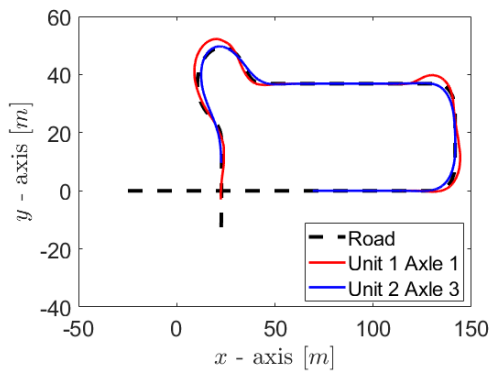
(b)  $PL_{linear}$  :  $d_{R11}$  and  $d_{R23}$



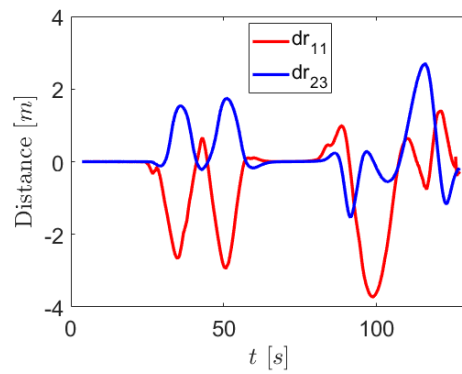
(c)  $PL_{kinematic}$  : Road tracking



(d)  $PL_{kinematic}$  :  $d_{R11}$  and  $d_{R23}$



(e)  $PLL_{linear}$  : Road tracking



(f)  $PLL_{linear}$  :  $d_{R11}$  and  $d_{R23}$

**Figure 5.13:** Real time simulation using HF model, Forces Pro solver and ROS: Road tracking,  $d_{R11}$  and  $d_{R23}$ .

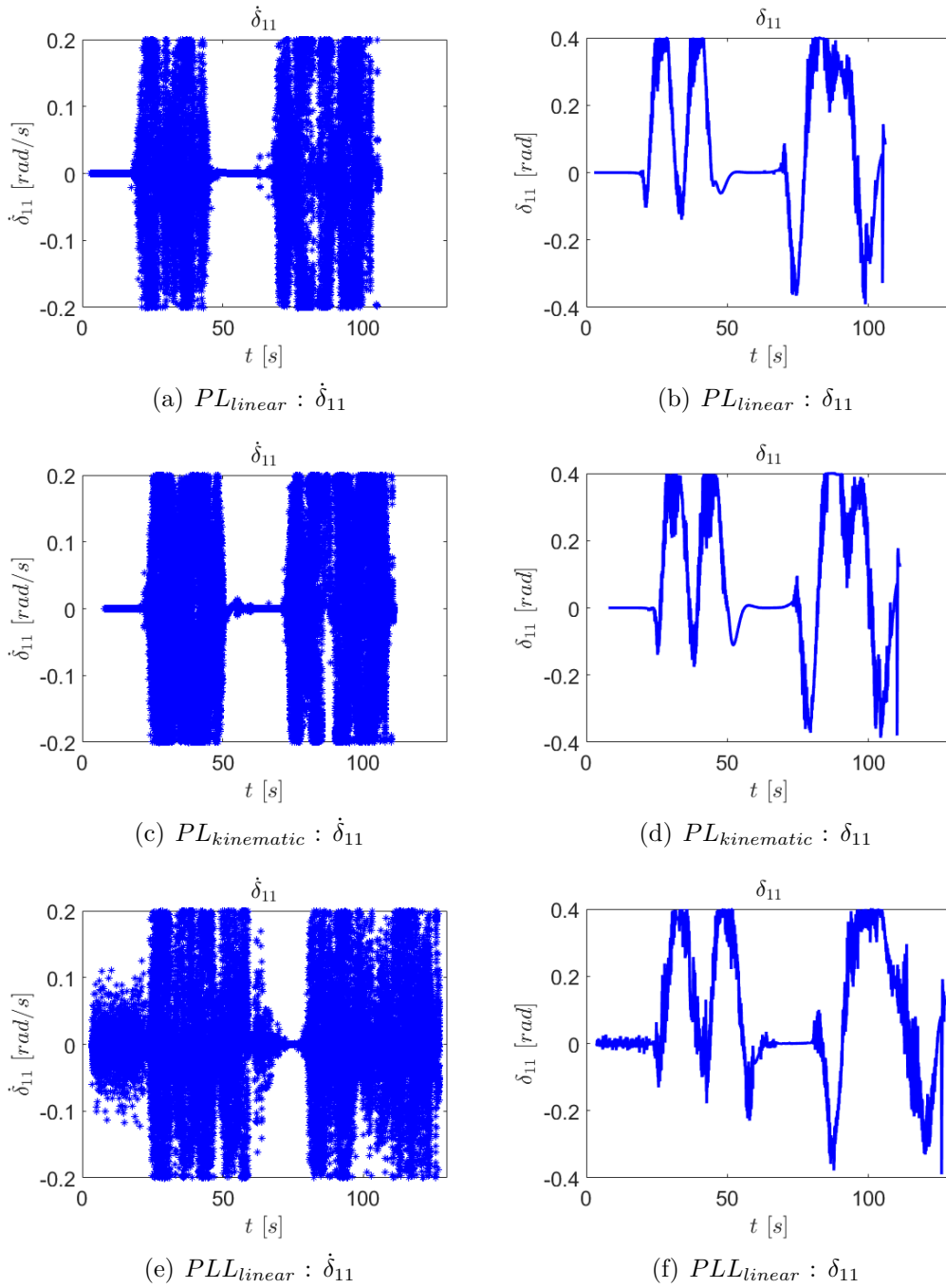
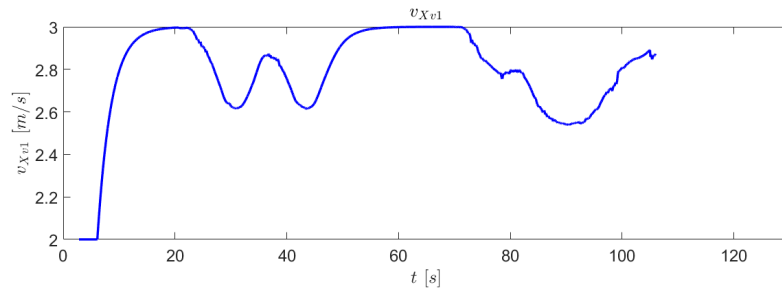
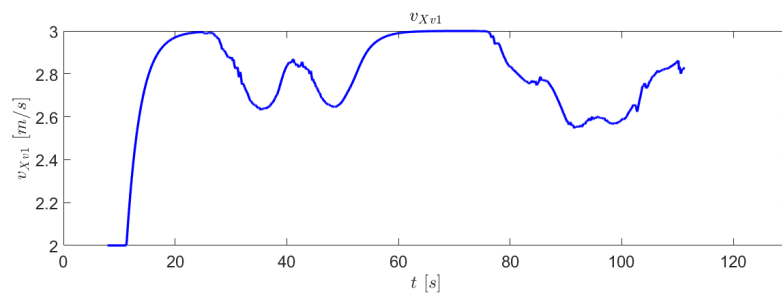


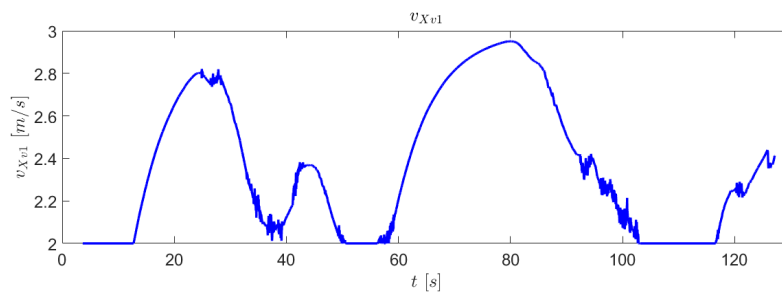
**Figure 5.14:** Real time simulation using HF model, Forces Pro solver and ROS:  $\delta_{11}$  and  $\dot{\delta}_{11}$ .



(a)  $PLL_{linear} : v_{Xv1}$



(b)  $PLL_{kinematic} : v_{Xv1}$



(c)  $PLL_{linear} : v_{Xv1}$

**Figure 5.15:** Real time simulation using HF model, Forces Pro solver and ROS : Longitudinal velocity  $v_{Xv1}$ .

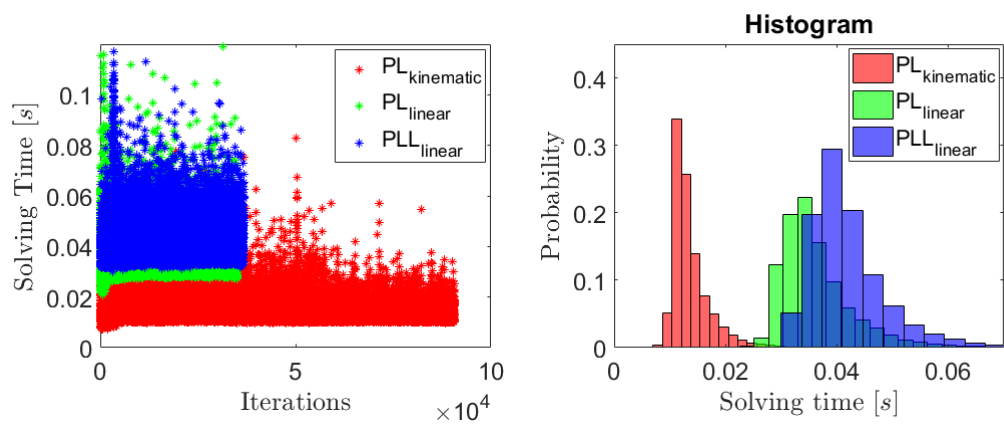


**Figure 5.16:** Real time simulation using HF model, Forces Pro and ROS: Planner solving time.



# 6

## Conclusions and Future work

### 6.1 Conclusions

In this section, the conclusions obtained by the three trajectory planners will be presented. The conclusions are related to the estimation errors of each model, the solving time of each planner, the operating velocities of the planners, the selection of the prediction horizon and the dependence of every planner on additional controllers.

In this thesis three different semi-trailer models are obtained: Linear model of lateral dynamics, Linear model of longitudinal and lateral dynamics and kinematic model. Low error estimation is observed in the three cases. The highest error is observed in the kinematic model, however its formulation is much simpler than the other two models.

In addition, three different planners are formulated using the three models obtained as equality constraints:  $PL_{linear}$ ,  $PL_{kinematic}$  and  $PLL_{linear}$ .  $PL_{kinematic}$  is the fastest planner (lowest solving time) and  $PLL_{linear}$  the slowest (highest solving time). It should be noted that the solving time can be influenced by several factors. These factors are the gains of the cost function, the hard inequality constraints, the complexity of the equality constraints, the prediction horizon, the number of the optimization variables, the discretization method, the time step as well as the number of times that the solution search algorithm is repeated to solve the optimization problem. By comparing all the trajectory planners, it should be noted that  $PLL_{linear}$  and  $PL_{linear}$  are more general, as they can operate at both high and small velocities. On the other hand,  $PL_{kinematic}$  can perform well at low velocities. Also, even though  $PL_{kinematic}$  and  $PL_{linear}$  are designed to operate at constant velocities, they can account for small deviations. This can be verified from the trajectory planners' results with HF model. Long prediction horizons would, in theory, increase the stability of the system. Though, as the trajectory planners use approximated to the HF models, using too long prediction horizons might lead to bad behavior. This can be explained by the increased with time estimation errors (model validation). As a result, the simplified models cannot be trusted for a long time. It should be noted that in order to use  $PL_{kinematic}$  and  $PL_{linear}$ , an additional longitudinal controller is needed. On the other hand, when using planner  $PLL_{linear}$ , no additional controller is needed.

### 6.2 Future work

Even though the trajectory planners performed in a good manner, several improvements can be suggested for future work. Suggestions on how to improve the trajectory planners' performance (generated trajectories and driving comfort), the accuracy of the models and the way the road characteristics are used, will be shown in the text below.

Firstly, it would be desirable to harden the constraint of lateral distance offset perpendicular to the road on the first axle to 2.5 m. In order for the trajectory planners to generate smooth trajectories and not to violate this constraint, different tuning is required. Hence, it is recommended to reformulate the optimization problem (without decreasing the prediction horizon) and improve the performance of the trajectory planners. However, neither of the trajectory planners considered minimizing or constraining the longitudinal or lateral jerk. Keeping the jerk in low values could lead to more comfortable driving.

Furthermore, there are several suggestions on how to increase the accuracy of the models. Including the aerodynamic drag and gravitational forces into the model could lead to more robust performance. Hence, it is recommended to design and test trajectory planners which can operate successfully on more realistic scenarios (e.g. strong wind, uphill road). Also, in this research, the Euler method is used to discretize the continuous systems. Since this method is in general poor, it is recommended to try and obtain good performance using higher-order methods, such as Runge-Kutta 2,3 and 4.

Lastly, instead of using sigmoid functions to describe the road characteristics (curvature and angle of the road) as functions of the covered distance, the road characteristics could be read from a look-up table. A way to achieve this is to predict the road characteristics in each time instance using the predicted cover distances from the previous solution of the optimization problem, which will be then applied on a look-up table. This method is easier to apply on different road scenarios as well as it may influence the overall performance of the trajectory planners.

# Bibliography

- [1] P. Nilsson, Traffic situation management for driving automation of articulated heavy road transports - from driver behaviour towards highway autopilot, Ph.D. thesis, Department of Mechanics and Maritime Sciences, Chalmers University of Technology, Sweden, 2017.
- [2] A. J. Hawkins. Toyota's self-driving cars can now fit more junk in their trunks. January 3, 2019. <https://www.theverge.com/2019/1/3/18166854/toyota-self-driving-car-test-vehicle-ces-2019>. Accessed 3 June, 2019.
- [3] A. Macduff and R. Aron. Autonomous trucks in real operation. February 20, 2019. <https://www.volvotrucks.com/en-en/news/volvo-trucks-magazine/2019/feb/bronnay.html>. Accessed 3 June, 2019.
- [4] L. Papadopoulos. Renault's new car is a shared self-driving all-electric luxury dream. October 4, 2018. <https://interestingengineering.com/renaults-new-car-is-a-shared-self-driving-all-electric-luxury-dream>. Accessed 3 June, 2019.
- [5] Self-Driving Cars Explained. February 21, 2018. <https://www.ucsusa.org/clean-vehicles/how-self-driving-cars-work>. Accessed 3 June, 2019.
- [6] Human Error Causes 94 Percent of Car Accidents. June 9, 2017. <https://blog.lawinfo.com/2017/09/06/human-error-causes-94-percent-of-car-accidents/>. Accessed 3 June, 2019.
- [7] Autonomous vehicles and the environment. August 6, 2018. <https://teleroute.com/en-en/blog/article/autonomous-vehicles-the-environment/>. Accessed 3 June, 2019.
- [8] M. Hutson. Watch just a few self-driving cars stop traffic jams. November 16, 2018. <https://www.sciencemag.org/news/2018/11/watch-just-few-self-driving-cars-stop-traffic-jams>. Accessed 3 June, 2019.
- [9] Volvotrucks.com. <https://www.volvotrucks.com/en-en/home.html>. Accessed 3 June, 2019.
- [10] D.G. Bautista and V. Milanes and J. Pérez and F. Nashashibi, Review of motion planning techniques for automated Vehicles, IEEE Transactions on Intelligent Transportation Systems, November 2015.
- [11] Julia Nilsson *Trajectory Planning via Convex Optimization in the Model Predictive Control Framework*. Department of Signals and Systems Chalmers University of Technology Goteborg, Sweden 2016.
- [12] R. Kala and K. Warwick, *Multi-level planning for semi-autonomous vehicles in traffic scenarios based on separation maximization*, J. Intell. Robot. Syst., vol. 72, no. 3/4, pp. 559–590, Dec. 2013.

- [13] M. Likhachev and D. Ferguson, *Planning long dynamically feasible maneuvers for autonomous vehicles*, Int. J. Robot. Res., vol. 28, no. 8, pp. 933–945, Aug. 2009.
- [14] O. Ljungqvist<sup>1</sup> and D. Axehill<sup>1</sup> and J. Lofberg, *On stability for state-lattice trajectory tracking control*, 2018 American Control Conference (ACC), Milwaukee, June 2018.
- [15] Y. Kuwata et al., *Real-time motion planning with applications to autonomous urban driving*, IEEE Trans. Control Syst. Technol., vol. 17, no. 5, pp. 1105–1118, Sep. 2009
- [16] B. Park and Y. Lee and W. Han *Trajectory generation method using Bezier spiral curves for high-speed on-road autonomous vehicles* 2014 IEEE International Conference on Automation Science and Engineering (CASE) Taipei, Taiwan, August 18-22, 2014.
- [17] L. Labakhua, U. Nunes, R. Rodrigues, and F. S. Leite *Smooth Trajectory Planning for Fully Automated Passengers Vehicles: Spline and clothoid based methods and its simulation* in Informatics in Control Automation and Robotics. Berlin, Germany: Springer-Verlag, 2008, pp. 169–182.
- [18] W. Lim and S. Lee and M. Sunwoo and K. Jo *Hierarchical trajectory planning of an autonomous car based on the integration of a sampling and an optimization method* IEEE transactions on intelligent transportation systems, vol. 19, no. 2, February 2018.
- [19] Q. T. Dinh\* and M. Diehl *An application of sequential convex programming to time optimal trajectory planning for a car motion* Joint 48th IEEE conference on decision and control and 28th Chinese control conference Shanghai, P.R. China, December 16-18, 2009.
- [20] C. Law, Off-tracking: how rear truck tires can crush pedestrians. <https://www.truckingwatchdog.com/2018/09/01/off-tracking-semi-truck/>. Accessed 3 June, 2019.
- [21] D. Gonzalez Bautista and V. Milanés and J. Pérez - F. Nashashibi. A Review of Motion Planning Techniques for Automated Vehicles, IEEE Transactions on Intelligent Transportation Systems, November 2015.
- [22] P. Wallin and P. Nilsson. Trajectory planning for automated highway driving of articulated heavy vehicles, Department of Electrical Engineering, Chalmers university of technology, 2018.
- [23] N. J. van Duijkeren, Real-time receding horizon trajectory generation for long heavy vehicle combinations on highways, Faculty of Mechanical, Maritime and Materials Engineering (3mE), Delft University of Technology, Netherlands, 2014.
- [24] A. Kalose. Controller for Steering of Smart Dolly, HAN University, 2018.
- [25] N. Andren and A. Gil Martín and K. Hoogendijk and L. Niklasson and F. Sandblom - F. Slottner Seholm. Predictive Control for Autonomous Articulated Vehicles, Department of Computer Science, Chalmers university of technology, 2017.
- [26] N. van Duijkeren and T. Keviczky and P. Nilsson and L. Laine, KU Leuven. Real-Time NMPC for Semi-Automated Highway Driving of Long Heavy

- Vehicle Combinations, Delft University of Technology, Volvo Group Trucks Technology.
- [27] M. S. Bazaraa, H. D. Sherali and C. M. Shetty, *Nonlinear programming*, Third Edition, John Wiley & Sons, 2006.
- [28] N. Andréasson, A. Evgrafov and M. Patriksson, *An Introduction to Continuous Optimization: Foundations and Fundamental Algorithms*, Third Edition, Studentlitteratur, 2016.
- [29] Ogata, Katsuhiko. *Modern Control Engineering*. Upper Saddle River, N.J: Prentice Hall, 1997.
- [30] Åström, Karl Johan and Richard M. Murray, *Feedback Systems : An Introduction for Scientists and Engineers*, Princeton University Press, Princeton and Oxford, 2012.
- [31] H. Kwakernaak and R. Sivan, *Linear Optimal Control Systems*, First Edition, John Wiley & Sons, 1972.
- [32] Rawlings, J. B., *Tutorial Overview of Model Predictive Control*, IEEE Contr. Syst. Magazine, 2000.
- [33] Rawlings, J. B., E. S. Meadows and K. R. Muske, *Nonlinear Model Predictive Control: A Tutorial and Survey*, Proc. Int. Symp. Adv. Control of Chemical Processes, p. 185, 1994.
- [34] Mayne, D. Q., J. B. Rawlings, C. V. Rao, and P. O. M. Scokaert, *Constrained Model Predictive Control: Stability and Optimality*, Automatica, 26(6), pp. 789 - 814, 2000.
- [35] L. Grüne and J. Pannek, *Nonlinear Model Predictive Control: Theory and Algorithms*, Springer Publishing Company, Incorporated, 2013
- [36] H. Sira-Ramirez, R. Ortega and G. Escobar, *Lagrangian Modeling of Switch Regulated DC-to-DC Power Converters*, IEEE Conference on Decision and Control, Kobe, Japan, December 1996, pp. 396-402.
- [37] H. A. Yildiz and L. Goren-Sumer, *Lagrangian modeling of DC-DC buck-boost and flyback converters*, Circuit Theory and Design 2009. ECCTD 2009. European Conference on, pp. 245-248, 2009.
- [38] K. U. Lee, H. S. Kim, J. B. Park and Y. H. Choi, *Hovering control of a quadrotor*, Proc. 121 International Conference on Control, Automation and Systems (ICCAS), pp. 162-167, 2012.
- [39] D. B. Tank, R. S. Jo and H. S. Jo, *Dynamic modelling and control of self-balancing one-legged robot*, IEEE International Conference on Automatic Control and Intelligent Systems, pp. 19 - 23, 2018.
- [40] D. d. Bruin, *Lateral Guidance of All-Wheel Steered Multiple-Articulated Vehicles*. Dissertation, Technische Universiteit Eindhoven, 2001.
- [41] C. Fletcher, C. Manzie, and M. Good, *Trailer Steering: An Australian Research Perspective and Application for By-Wire Control*. Technical report, Ninth International Symposium on Heavy Vehicle Weights and Dimensions. June 18-22, Penn State, State College, Pennsylvania, 2006.
- [42] M. K. Bahaghighat, S. Kharrazi, M. Lidberg, P. Falcone and B. Schofield, *Predictive Yaw and Lateral Control in Long Heavy Vehicles Combinations*, IEEE Conference on Decision and Control, pp. 6403-6408, 2010.

- [43] C. Chen and M. Tomizuka, Dynamic Modeling of Tractor-Semitrailer Vehicle in Automated Highway Systems, California Path Program Institute of Transportation studies, University of California, Bekerley, 1995.
- [44] Z. Yu and J. Li, Modeling and verification of heavy-duty semi-trailer, International Conference on Transportation, Mechanical, and Electrical Engineering (TMEE), pp. 982 - 985, 2011.
- [45] H. B. Pacejka. Tire and vehicle dynamics. Butterworth-Heinemann, 2006.
- [46] P. Nilsson, K. Tagesson, Single-track models of an a-double heavy vehicle combination, Tech. rep., Department of Applied Mechanics, Chalmers University of Technology, Sweden, 2013.
- [47] B. Jacobson. Vehicle Dynamics - Compendium for Course MMF062. Chalmers University of Technology, 2016.
- [48] Trafikverket, Krav för vägars och gators utformning, 2015.
- [49] D. S. Meek and R. Thomas, A guided clothoid spline. Computer Aided Geometric Design 8.2, pp. 163-174, 1991.
- [50] J. Stoer, Curve fitting with clothoidal splines, J. Res. Nat. Bur. Stand., 87, pp. 317-346, 1982.
- [51] J. Aurell and T. Wadman, Vehicle combinations based on the modular concept. Tech. rep. 1. NVF-reports, Report 1/2007, 2007. DOI: ISSN:0347-2485.
- [52] T. D. Gillespie and C. B. Winkler, On the directional response characteristics of heavy vehicles, The Dynamics of Vehicles on Roads and Tracks, Amsterdam, Swets&Zeitlinger, pp. 165- 187, 1978.
- [53] C. B. Winkler. Simplified Analysis of the Steady-State Turning of Complex Vehicles, Vehicle System Dynamics 29, pp. 141-180, 1998.
- [54] S. S. Institute. SS-ISO 8855:2011. Road vehicles - Vehicle dynamics and road-holding ability - Vocabulary. 2011.
- [55] A. Boström, Rigid body dynamics, Chalmers University of Technology, 2012.
- [56] B. Siciliano, L. Sciavicco, L. Villani and G. Oriolo, Robotics: Modelling, Planning and Control, Springer Publishing Company, 2008.
- [57] P. Nilsson, K. Tagesson, Single-track models of an a-double heavy vehicle combination, Tech. rep., Department of Applied Mechanics, Chalmers University of Technology, Sweden, 2013.
- [58] R. Kusumakar, K. Kural, A. S. Tomar and B. Pyman, Autonomous parking for articulated vehicles, HAN University of Applied Science, Netherlands, 2017.
- [59] J. Pauwelussen, Essentials of vehicle dynamics, Butterworth-Heinemann, 2014.
- [60] R. Werner, S. Mueller, and G. Kormann, Path tracking control of tractors and steerable implements based on kinematic and dynamic modeling, in Proc. 11th Int. Conf. Precis. Agricult., pp. 15–18, 2012.
- [61] B. A. Jujnovich and D. Cebon, Path-following steering control for articulated vehicles, J. Dyn. Syst., Meas. Control, vol .135, no. 3, 2013.



# A

## Nomenclature

$\{E\}$	: Earth fixed frame.
$\{1\}$	: Vehicle unit 1 body fixed frame.
$\{2\}$	: Vehicle unit 2 body fixed frame.
$\{W\}$	: Vehicle unit 1 axle 1 wheel fixed frame.
$\mathcal{N}_u = \{1, 2\}$	: Set of number of vehicle units.
$\mathcal{N}_a = \{1, 2, 3\}$	: Set of number of axles.
$\delta_{11}$	: Steering angle of vehicle unit 1 axle 1.
$\psi_j$	: Yaw angle of vehicle unit $j$ ;
$\Delta\psi_1$	: Articulation angle of the trailing vehicle unit 1;
$(X_E, Y_E)$	: Earth fixed frame.
$(X_{W11}, Y_{W11})$	: Unit 1 wheel 1 fixed frame.
$(X_{Vj}, Y_{Vj})$	: Vehicle unit $j$ body fixed frame;
$(x_j, y_j)$	: Center of gravity of vehicle unit $j$ ;
$v_{Xvj}$	: The $x$ -axis component of the translational velocity vector of vehicle unit $j$ in a body fixed frame;
$v_{Yvj}$	: The $y$ -axis component of the translational velocity vector of vehicle unit $j$ in a body fixed frame;
$l_{jk}$	: Distance from center of gravity of unit $j$ to axle $k$ ;
$l_{jc1}$	: Distance from center of gravity of unit $j$ to the connection point rear of unit 1;
$F_{Xwj k}$	: The $x$ -axis component of tyre force of vehicle unit $j$ axle $k$ in a wheel fixed frame;
$F_{Ywj k}$	: The $y$ -axis component of tyre force of vehicle unit $j$ axle $k$ in a wheel fixed frame;
$F_{grav,j}$	: Gravitational force of vehicle unit $j$ ;
$F_{air}$	: Aerodynamic drag in a body fixed frame;
$r_j$	: Position vector for center of gravity of vehicle unit $j$ with respect to earth frame;
$r_{jk}$	: Position vector of vehicle unit $j$ axle $k$ with respect to earth frame;
$r_{jk}^j$	: Position vector of vehicle unit $j$ axle $k$ with respect to frame $j$ ;
$r_{jc1}$	: Position vector of vehicle unit $j$ axle $k$ with respect to earth frame;
$r_{jc1}^j$	: Position vector of vehicle unit $j$ axle $k$ with respect to frame $j$ ;